Article, Discoveries

A Phylogenomic Assessment of Processes Underpinning Convergent Evolution in Open-Habitat Chats

Niloofar Alaei Kakhki [1], Manuel Schweizer [2,3], Dave Lutgen [3,1,4], Rauri C. K. Bowie [5,6], Hadoram Shirihai [2], Alexander Suh [7,8], Holger Schielzeth [1,9], Reto Burri [4,3,1]

[1] Department of Population Ecology, Institute of Ecology and Evolution, Friedrich-Schiller-University Jena, Jena, Germany

[2] Natural History Museum Bern, Bern, Switzerland

[3] Institute of Ecology and Evolution, University of Bern, Bern, Switzerland

[4] Swiss Ornithological Institute, Sempach, Switzerland

[5] Museum of Vertebrate Zoology, University of California, Berkeley, USA

[6] Department of Integrative Biology, University of California, Berkeley, USA

[7] School of Biological Sciences, University of East Anglia, Norwich, United Kingdom

[8] Department of Organismal Biology – Systematic Biology (EBC), Science for Life Laboratory, Evolutionary Biology Centre, Uppsala University, Uppsala, Sweden

[9] German Centre for Integrative Biodiversity Research (iDiv), Halle-Jena-Leipzig, Leipzig, Germany

Correspondence

Niloofar Alaei Kakhki, Department of Population Ecology, Institute of Ecology and Evolution, Friedrich-Schiller-University Jena, Dornburger Str. 159, D-07743 Jena, Germany
Email: niloofar.alaei.kakhki@uni-jena.de

Reto Burri, Swiss Ornithological Institute, Seerose 1, CH-6204 Sempach.
Email: reto.burri@vogelwarte.ch

Abstract

Insights into the processes underpinning convergent evolution advance our understanding of the contributions of ancestral, introgressed, and novel genetic variation to phenotypic evolution. Phylogenomic analyses characterizing genome-wide gene tree heterogeneity can provide first clues about the extent of ILS and of introgression and thereby into the potential of these processes or (in their absence) the need to invoke novel mutations to underpin convergent evolution. Here, we were interested in understanding the processes involved in convergent evolution in open-habitat chats (wheatears of the genus *Oenanthe* and their relatives). To this end, based on whole-genome resequencing data from 50 taxa of 44 species, we established the species tree, characterized gene tree heterogeneity, and investigated the footprints of ILS and introgression within the latter. The species tree corroborates the pattern of abundant convergent evolution, especially in wheatears. The high levels of gene tree heterogeneity in wheatears are explained by ILS alone only for 30% of internal branches. For multiple branches with high gene tree heterogeneity, D-statistics and phylogenetic networks identified footprints of introgression. Finally, long branches without extensive ILS between clades sporting similar phenotypes provide suggestive evidence for a role of novel mutations in the evolution of these phenotypes. Together, our results suggest that convergent evolution in open-habitat chats involved diverse processes and highlight that phenotypic diversification is often complex and best depicted as a network of interacting lineages.

Introduction

Molecular phylogenetics has unveiled many previously unknown examples of convergent evolution – here meant to refer to a *phenotypic pattern* in which non-sister species are phenotypically more similar to each other than to their respective sister species (following Arendt and Reznick 2008; Stern 2013). Under such an evolutionary outcome, species relationships based on morphometrics, coloration, behavior, or other ecological traits are discordant with the history of descent reflected in the species tree (Aliabadian et al. 2012; Elmer and Meyer 2011; Jarvis et al. 2014; Martin and Orgogozo 2013; Paterson et al. 2020; Schweizer et al. 2019a; Schweizer et al. 2019b; Stern 2013). While the many observations of such discordances across the tree of life witness of the abundance of convergent evolution, insights into the underlying processes remain more elusive.

Phylogenetic information from genomic data now provides unprecedented power to consolidate patterns of convergent evolution and obtain insights into the underlying processes. Many examples of putative convergent evolution are yet based on phylogenies reconstructed from a restricted number of genetic markers (Aliabadian et al. 2012; Brusatte et al. 2015; Colosimo et al. 2005; Cresko et al. 2004; Stern 2013). Since phylogenetic relationships at different positions in

64 the genome, referred to as 'gene trees', can vary substantially, many gene trees inevitably deviate
65 from the species' history of descent reflected in the species tree (Degnan and Rosenberg 2006;
66 Toews and Brelsford 2012). Hence, the mismatch of single gene trees with phenotypic similarities
67 alone does not provide conclusive evidence for convergent evolution (Degnan and Rosenberg
68 2006; Doyle 1997; Lamers et al. 2012). Confirming instances of convergent evolution, therefore,
69 requires species tree reconstructions from genome-wide variation. Once the evidence for
70 convergent evolution is corroborated by the species tree, we can move forward to investigate the
71 processes underlying gene tree heterogeneity that may also underpin convergent evolution.

72 Convergent evolution can occur via three processes: First, phenotypic similarities can
73 evolve through independent mutations in the same or different genes ("parallel evolution" *sensu*
74 Stern 2013) (Arendt and Reznick 2008; Martin and Orgogozo 2013; Stern 2013). In Mexican
75 cavefish (*Astyanax mexicanus*), for instance, the evolution of decolored brown phenotypes and
76 albinism in separate caves occurred through different mutations in the MC1R and OCA2 genes
77 (Gross et al. 2009; Protas et al. 2006; Stahl and Gross 2015). Similarly, in plants, isoforms of PEPC
78 found in C4 photosynthesis, and similar floral traits important for pollination have evolved
79 multiple times independently (Besnard et al. 2009; Christin et al. 2007; Hoballah et al. 2007;
80 Preston and Hileman 2009; Whittall et al. 2006).

81 The second, and likely most frequent process leading to convergent evolution that also
82 accounts for most gene tree heterogeneity is incomplete lineage sorting (ILS; Stern 2013 includes
83 this under "collateral evolution"), that is, the retention of alleles and traits that were already
84 present in the ancestral lineage (Colosimo et al. 2005; Cresko et al. 2004; Stern 2013; Van
85 Belleghem et al. 2018). ILS is prevalent in radiations characterized by large effective population
86 sizes and fast succession of speciation events, such as in the evolution of neoavian birds (Jarvis et
87 al. 2014; Suh 2016; Suh et al. 2015) or in the diversification of sticklebacks (Colosimo et al. 2005;
88 Jones et al. 2012; Roberts Kingman et al. 2021). In such cases, a high proportion of ancestral
89 variation may be retained over subsequent species splits and segregate in the independently
90 segregating gene pools of daughter species (Maddison 1997). Selection or drift in non-sister
91 species may fix the same genotype (and phenotype), while sister species may fix a different
92 genotype/phenotype. For instance in Humans 1% of the genome is genetically more similar to
93 orangutans than to chimps due to ILS, even though these primates are characterized by small
94 effective population sizes (Hobolth et al. 2011).

95 Third, in hybridizing lineages, convergent evolution and gene tree heterogeneity may be
96 underpinned by introgression (the exchange of genetic material between species) that mingles
97 genotypes and phenotypes among species (Stern 2013 includes this under "collateral evolution")
98 (Heliconius Genome Consortium 2012; Malinsky et al. 2018; Song et al. 2011; Stryjewski and
99 Sorenson 2017). In particular, introgression between non-sister species may result in these

species being phenotypically more similar than they are to their respective sister species, such as exemplified by wing-pattern mimicry in *Heliconius* butterflies (Edelman et al. 2019; Pardo-Diaz et al. 2012), and by plumage coloration of *Munia* finches and of members of the Black-eared Wheatear (*Oenanthe hispanica*) complex (Schweizer et al. 2019a; Stryjewski and Sorenson 2017). Importantly, in an increasing number of instances, such as in *Heliconius* butterflies, Yellowstone wolves, Darwin's finches, and cichlid fish, introgression has exchanged alleles between species and resulted in the formation of beneficial phenotypes (Enciso-Romero et al. 2017; Genner and Turner 2012; Grant et al. 2005; Lamers et al. 2012; Wallbank et al. 2016). Given that over the last decade genomic studies have contributed increasing evidence for the abundance of such adaptive introgression, hybridization (the interbreeding of different species) may underpin convergent evolution more often than previously appreciated (Campagna et al. 2017; Han et al. 2017; Marques et al. 2019a; Meier et al. 2018).

Multiple factors influence which of these processes were most likely involved in specific cases of convergent evolution. These factors include the evolutionary time scale under consideration, the speed at which successive speciation events occurred, effective population sizes, and the opportunity for genetic exchange according to biogeographic history. Waiting times for beneficial mutations are long (Barrett and Schluter 2008; Hedrick 2013; Hermisson and Pennings 2005). Independent mutations with the same phenotypic effect are thus exceedingly rare (Eyre-Walker and Keightley 2007) and only over the course of millions of years may occur in sufficient number to be a source of convergent evolution (Hedrick 2013). Therefore, at short evolutionary time scales, convergent evolution may more often involve the recruitment of standing genetic variation (Barrett and Schluter 2008), notably from the pool of ancestral variation segregating in extant species, or variation introgressed from other species (Stern 2013); especially since in young lineages ancestral variation is still segregating and because reproductive isolation may still be incomplete between young species.

Phylogenomics can provide important indirect insights into the potential contribution of ILS, introgression, and novel mutations to convergent evolution: First, the species tree provides initial clues on whether speciation events occurred over short enough time scales for ancestral variation to be passed to descent lineages and thus remain incompletely sorted in important proportions beyond speciation events. Second, insights into the extent of ILS and presence of introgression can be gained from levels of gene tree heterogeneity (Degnan and Rosenberg 2006; Funk and Omland 2003; Jarvis et al. 2014; Nater et al. 2015; Suh 2016; Suh et al. 2015) and symmetries of gene tree frequencies (Hibbins and Hahn 2022). Gene tree heterogeneity is high under both ILS and introgression, but the two processes leave different proportions of alternative gene trees, based on which they can be distinguished (Hibbins and Hahn 2022; Sayyari and Mirarab 2018; Sayyari et al. 2018). In the presence of extensive ILS or of introgression, a

136 parsimonious approach attributes the source of convergent evolution to these processes, even
137 though independent mutations cannot be excluded as the source of convergent evolution
138 (Colosimo et al. 2005; Cresko et al. 2004; Pardo-Diaz et al. 2012; Stryjewski and Sorenson 2017).
139 The absence of detecting these processes, conversely, would indirectly suggest novel mutations
140 as a potential source of convergent evolution. Therefore, surveys of gene tree heterogeneity and
141 symmetries of gene tree proportions represent a promising avenue to probe the potential of the
142 alternative processes to contribute to convergent evolution.

143 Here, we reconstructed the species tree and assessed the contribution of ILS and
144 introgression to gene tree heterogeneity in open-habitat chats (genera *Campicoloides*,
145 *Emarginata, Myrmecocichla, Oenanthe*, *Pinarochroa* and *Thamnolaea*), a monophyletic group of
146 songbirds displaying a high incidence of convergent evolution (Aliabadian et al. 2012; Mayr and
147 Stresemann 1950; Schweizer et al. 2019a; Schweizer et al. 2019b). The phylogenetic relationships
148 among open-habitat chats inferred from mitochondrial data were entirely unexpected from a
149 morphological perspective (Aliabadian et al. 2012). Species similar in plumage coloration and
150 other traits were often spread far apart across the mitochondrial phylogeny, suggesting
151 convergent evolution of phenotypic similarities (Aliabadian et al. 2012; Outlaw et al. 2010;
152 Schweizer and Shirihai 2013; Schweizer et al. 2019a; Schweizer et al. 2019b). For a limited subset
153 of species studied, genome-wide variation (ddRAD data) confirmed the mitochondrial
154 relationships (Schweizer et al. 2019b). Furthermore, hybridization resulted in substantial
155 introgression in the *Oenanthe hispanica* complex (Schweizer et al. 2019a) and is suspected to have
156 played a role in phenotypic and species evolution in the *O. picata* complex (Panov 2005). In these
157 instances, introgression between non-sister taxa may well explain convergent evolution.
158 However, genomic data is essential to corroborate and refine the species tree and assess the
159 incidence of ILS and/or introgression across open-habitat chats.

160 Based on whole-genome resequencing data from 50 taxa of 44 open-habitat species (**Tab.**
161 **S1**), we aimed to obtain insights into the potential roles of alternative processes in driving
162 convergent evolution in these songbirds. To this end, we (i) reconstructed the species tree, (ii)
163 estimated gene tree variation across the genome, and (iii) explored ILS and introgression as
164 drivers of the underlying high gene tree heterogeneity. Our results reveal a comprehensive picture
165 of open-habitat chat evolution involving high rates of ILS and multiple instances of introgression
166 particularly in wheatears (genus *Oenanthe*). Footprints of ILS and introgression as well as
167 considerable divergence times between the main clades of wheatears with convergent evolution
168 suggest that, most likely, a combination of ILS, introgression, and novel mutations explains the
169 convergent evolution observed in wheatears.

170

171 # Results

172 ## Sampling, Nuclear Data Preparation, and Mitogenome Assembly

173 To achieve an almost complete taxon sampling, we resequenced the genomes of 50 open-habitat
174 chat taxa from 44 of 47 recognized species (**Fig. 1**; **Tab. S1**). A *Saxicola maurus* genome was
175 included as outgroup (Sangster et al. 2010; Zuccon and Ericson 2010). We mapped the sequencing
176 reads to the reference genome assembly of *Oenanthe melanoleuca* (Peona et al. in prep.) and
177 followed GATK best practices for nuclear data preparation. Mapping efficiency was not correlated
178 with the degree of divergence from the reference genome, but data obtained from DNA extracted
179 off museum skins mapped at a lower percentage (linear model, d_{XY}: t=-0.41, p=0.68; $tissue_{museum}$:
180 t=-6.56, p<0.001; R^2=0.53). After mapping, sequencing coverage ranged from 4.6 x to 40.6 x, with
181 an average coverage of 12.2 x ± 6.2 x (**Tab. S1**). We extracted mitochondrial sequence data for all
182 13 protein-coding genes and two rRNA genes from the resequencing data using MitoFinder 1.2
183 (Allio et al. 2020). To ensure that results did not depend on filtering strategy, all analyses were
184 run with four sets of differently filtered data (see Material and Methods).

185 ## Species Tree Reconstruction Based on Nuclear Genomic Data

186 We first set out to reconstruct and root the species tree based on regions of the genome least likely
187 affected by mapping biases. To this end, we extracted data from genomic intervals hosting avian
188 Benchmarking Universal Single-Copy Orthologs (BUSCO). This resulted in data from 7,335 BUSCO,
189 with alignment lengths varying from 89,898 kb to 140,640 kb (depending on filtering strategy)
190 for ML analyses of concatenated data, respectively 2,091 BUSCO with alignment lengths varying
191 from 10,575 kb to 15,290 kb for LD-pruned data free of interlocus recombination for multispecies
192 coalescent-based species tree reconstruction. Results were consistent among filtering strategies.
193 Hence, we only report results based on the most stringent filtering of read depth (ii, DP=5,
194 PW=50%, MD=15%). Both, maximum likelihood (ML) analyses in IQtree2 based on concatenated
195 data and multi-species coalescent analyses in ASTRAL-III (based on BUSCO ML gene trees)
196 established sub-Saharan species of the genera *Campicoloides*, *Emarginata*, *Myrmecocichla*,
197 *Pinarochroa*, and *Thamnolaea* as the sister clade to all other open-habitat chats (**Fig. S1a**). For the
198 subsequent analyses we excluded the *Saxicola* outgroup and rooted the trees on the sub-Saharan
199 clade.

200 We then moved to reconstruct the species tree based on an as broad representation of the
201 genome as possible. To this end, we extracted alignments including variant and invariant sites for
202 non-overlapping 10 kb windows. We henceforth refer to these windowed data as "loci". Analyses
203 included only loci that fulfilled filtering criteria for read depth, alignment length, data missingness
204 (see Material and Methods), and absence of evidence for intra-locus recombination. Furthermore,
205 we sub-sampled filtered loci to be at least 10 kb apart to ensure free inter-locus recombination.

206 Depending on filtering strategy, this left us with 5,267-6,791 loci with total alignment lengths of
207 34,556-52,243 kb (**Tab. S2**). We identified branches in the "anomaly zone" (Degnan and
208 Rosenberg 2006) in several clades of wheatears: in the *hispanica* and *picata* complexes, and in the

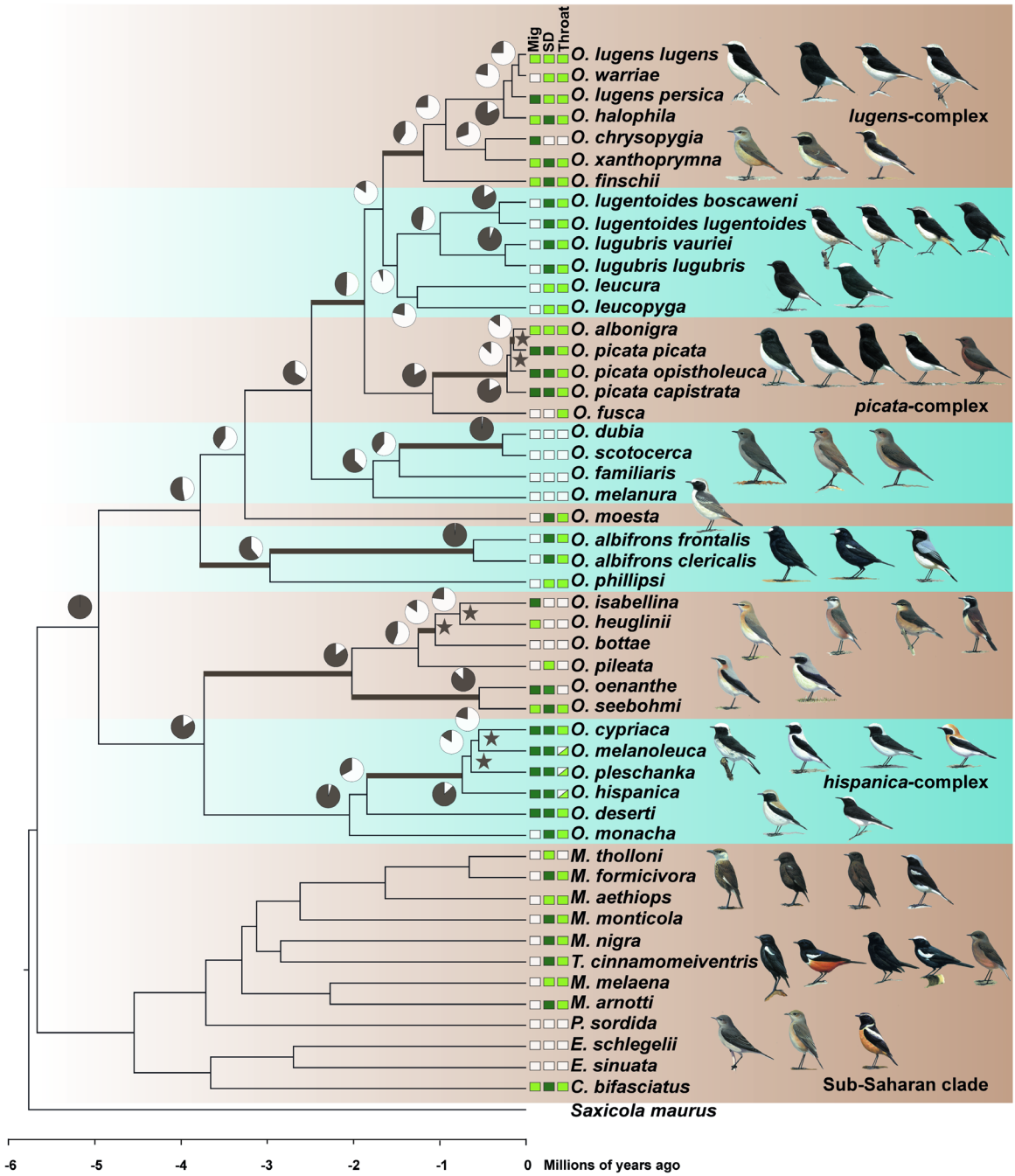

Figure 1 | Time-calibrated phylogenetic tree of open-habitat chats and levels of ILS. All nodes are supported by bootstrap values of 100. Pie charts depict the gene tree heterogeneity for each internal branch, with the brown proportion indicating the proportion of concordant gene trees (gCF). Coloured branches indicate internal branches for which ILS alone is statistically sufficient to explain the observed gene tree heterogeneity. Stars indicate branches that are in the phylogenetic anomaly zone. The character states of three selected characters: Sexual dimorphism (SD), monomorphic female-type (white), monomorphic male-type (pale green), dimorphic (dark green); Migratory behaviour (Mig), sedentary (white), short-distance migrant (pale green), long-distance migrant (dark green); and throat coloration (throat), white (white), black (pale green), and polymorphic (white and pale green). Drawing courtesy of Chris Rose (www.chrisrose-artist.co.uk) with permission from Bloomsbury Publishing Plc.

209 *isabellina* clade **(Fig. 1)**. Nevertheless, the polytomy test based on local quartet supports in
210 ASTRAL-III showed no evidence for polytomies in the species tree (P = 0 for all branches). The ML
211 tree based on concatenated data and the multi-species coalescent-based species tree were fully
212 supported and in agreement both with each other (except the position of T. *cinnamomeiventris*
213 within the sub-Saharan clade) and with the tree based on BUSCO (**Fig. S1b**). Finally, a SNP-based
214 species tree estimated in SVDquartets mostly confirmed the sequence-based results (**Fig. S2**). The
215 only three disagreements (position of *O. leucura* and *O. leucopygia,* position of *O. bottae* and *O.*
216 *pileata*, and position of *T. cinnamomeiventris*) were poorly supported in the SNP-based analysis
217 and are likely a result of high levels of ILS under which sequence-based approaches are more
218 accurate than approaches based on SNP data alone (Chou et al. 2015).

219 **Mitogenomic Relationships and Mito-Nuclear Discordances**

220 We were interested in whether previously inferred relationships based predominantly on single
221 mitochondrial genes (Alaei Kakhki et al. 2016; Aliabadian et al. 2012; Schweizer and Shirihai
222 2013) were supported by full mitogenomes and in inferring mito-nuclear discordances.

223 Mitogenomic relationships were in remarkable agreement with previously inferred
224 phylogenetic relationships based predominantly on individual mitochondrial genes (Alaei Kakhki
225 et al. 2016; Aliabadian et al. 2012; Schweizer and Shirihai 2013), yet showed several discordances
226 with the species tree recovered from nuclear data (**Fig. 2**). Mito-nuclear discordances in
227 wheatears were found in several places across the species tree but were mostly restricted to the
228 placements of tip taxa: (i) In the *lugens* complex, nuclear data placed *O. l. persica* within the
229 complex, whereas the mitogenome placed it with *O. xanthoprymna* and *O. chrysopygia.* (ii) In the
230 *picata* complex, *O. albonigra* that by mitochondrial data was considered a sister taxon to the *picata*
231 complex, was placed within the latter as a sister taxon to the phenotypically almost identical *O. p.*
232 *picata* by nuclear data. (iii) In the *hispanica* complex, *O. cypriaca* was placed as sister to either *O.*
233 *melanoleuca* or *O. pleschanka* in nuclear and mitogenomic data respectively. (iv) In the *isabellina*
234 clade, *O. heuglini* as sister to either *O. isabelline* or *O. bottae* by nuclear or mitogenomic data,
235 respectively. (v) Moreover, *O. leucura* and *O. leucopyga* formed a sister clade to the *O.*
236 *lugubris/lugentoides* clade according to the nuclear species tree, but mitogenomes placed them
237 consecutively at the root of the clade including *O. finschi* and the *lugens* complex. To understand
238 whether nuclear gene trees were entirely discordant with mitogenomic relationships or in part
239 reflected the latter, for each of the above discordances we checked for nuclear gene trees that
240 agreed with the mitogenomic tree. This showed that for most of the mitonuclear discordances,
241 roughly 15% of the gene trees agreed with the mitogenomic relationships (*picata* complex:
242 14.40%, 4,282 of 29,730 gene trees; *hispanica* complex: 13.13%, 3,905 of 29,730 gene trees;
243 *isabellina* clade: 15.71%, 4,671 of 29,730 gene trees; *lugens* complex: 2.77%, 824 of 29,730 gene
244 trees).

Time trees

In addition to species' relationships, we were interested in understanding the time scales at which species diverged. Due to the lack of appropriate fossils, we resorted to first estimating a time-calibrated mitochondrial phylogeny based on the 13 mitochondrial protein-coding genes, for which substitution rates are available (Lerner et al. 2011). The analysis in BEAST 2.6.6 showed high convergence of all parameters in three independent runs after 25% of the trees were discarded as burn-in (ESS >300). The results were in good agreement with pervious results obtained from single genes (Alaei Kakhki et al. 2016), dating the origin of open-habitat chats to the Miocene about 5.67 million years ago (mya) (95% highest posterior density (HPD): 5.32–6.06 mya). The diversification of wheatears (genus *Oenanthe*) started about 5.09 mya (95% HPD: 4.75–5.44 mya) **(Fig. 1, Fig. S3).**

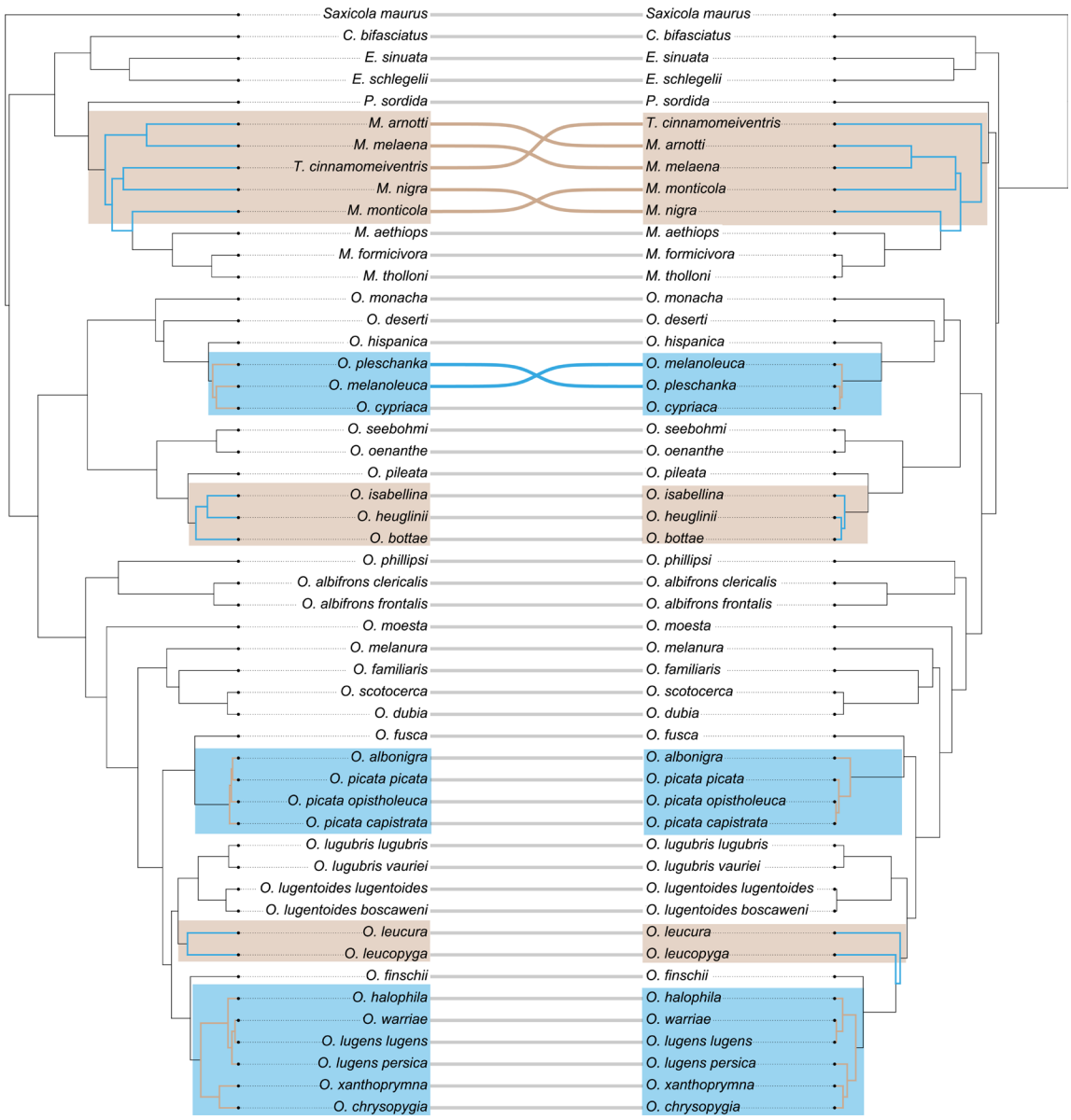

Figure 2 | Mito-nuclear discordances. Shown are the time-calibrated phylogenetic trees based on nuclear data (left) and full mitogenomes (right).

256 We then used the diversification time of the open-habitat chats estimated from
257 mitochondrial data as a time constraint in dating analyses based on nuclear data. For these
258 analyses, we first provided the topology and branch lengths obtained from ML analyses of
259 concatenated BUSCO data along with 1.8 Mb high-confidence nuclear data (see Material and
260 Methods) to generate the time-calibrated tree with RelTime-ML (Kumar et al. 2018). Compared
261 to the mitochondrial results, the nuclear data mostly estimated similar divergence times between
262 clades and shorter divergence times within clades (Pearson's r=0.93, p<0.001) (**Fig. 1, Fig. S3**).
263 Second, we performed dating analyses for windowed loci across the genome the same way as for
264 BUSCO by providing 3.8 Mb high-confidence data. Divergence times based on BUSCO strongly
265 correlated with ones estimated from windowed loci (Pearson's r=0.99, p<0.001) **(Fig. S4)**. A test
266 in which we re-ran the estimation of mitochondrial divergence times in RelTime-ML the same way
267 as for nuclear data yielded the same divergence times as estimated in BEAST, thus confirming that
268 differences in divergence times between mitochondrial and nuclear data are not due to the
269 approach but reflect the different data types.

270 **Extensive Gene Tree Heterogeneity**

271 Having established the species tree, we aimed to quantify the levels of gene tree heterogeneity in
272 wheatears to understand whether the processes generating gene tree heterogeneity could
273 underly convergent evolution in this core group of open-habitat chats that displays the highest
274 incidence of convergent evolution.

275 Several lines of evidence demonstrate extensive gene tree heterogeneity in wheatears.
276 Remarkably, not a single gene tree out of 29,730 gene trees matched the species tree.
277 Furthermore, many branches of the species tree – including ones with local posterior probability
278 1 – showed a high number of conflicting compared to concordant bipartitions, as evidenced by
279 low Internode Certainty All (ICA) scores (**Fig. S5**), with ICA ranging from 1 to 0.35 and average
280 ICA of 0.65 ± 0.19 (mean ± standard deviation). The high gene tree heterogeneities highlighted by
281 ICA were further supported by low percentages of gene trees recovering the topology of the
282 species tree at these internodes, as estimated by the gene concordance factor (gCF) (**Fig. 1**) that
283 ranged from 1 to 0.06 with an average of 0.52 ± 0.30 (mean ± standard deviation). ICA and gCF
284 were highly correlated (Pearson's r=0.94, p<0.001) **(Fig. S5)**. As expected, evidence for extensive
285 gene tree heterogeneity was highest in clades with branches classified as within the phylogenetic
286 anomaly zone. These included the *lugens*, *picata*, and *hispanica* complexes, the *isabellina* clade,
287 and the placement of *O. leucopyga* and *O. leucura.*

Contributions of ILS to Gene Tree Heterogeneity

Next, we aimed to understand to which extent the levels of gene tree heterogeneity observed in wheatears can be explained by ILS alone. To this end, we first tested whether the multi-species coalescent without hybridization adequately explains the gene tree heterogeneity observed across the entire species tree. The Tree Incongruence Checking in R (TICR) test (Stenz et al. 2015) showed an excess of outlier quartets ($p < 0.01$), indicating that a model including ILS but not introgression does not adequately explain the observed gene tree heterogeneity. This suggests that introgression occurred during the evolutionary history of wheatears.

Therefore, we moved on to infer for each branch in the species tree separately whether ILS alone may explain the level of gene tree heterogeneity. To this end, for each internal branch,

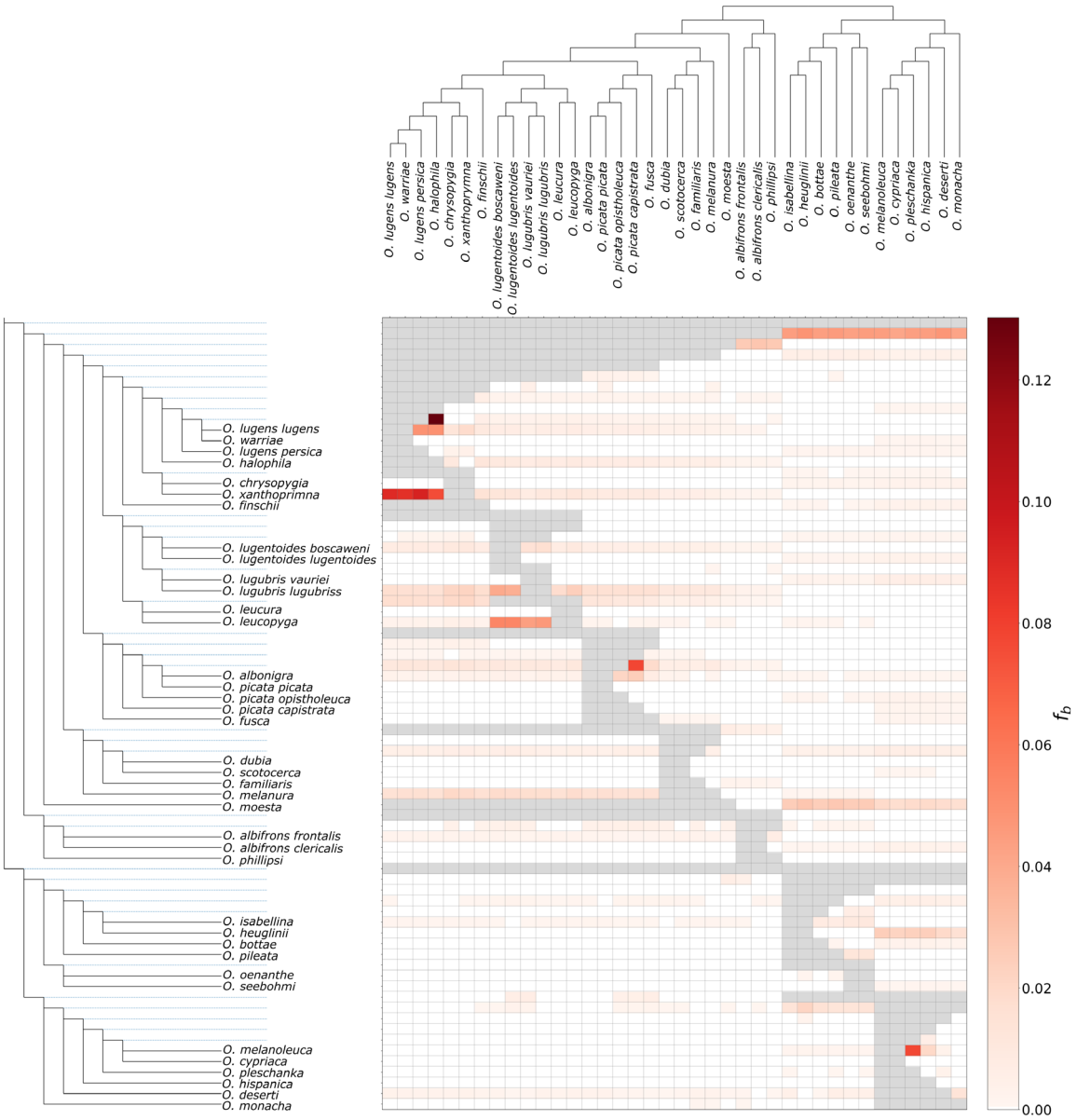

Figure 3 | Footprints of introgression as estimated by the f-branch statistic. The heat map summarizes the f-branch statistics estimated in Dsuite. Darker colors depict increasing evidence for gene flow between lineages. Dotted lines in the phylogeny represent ancestral lineage.

298 we estimated the number of gene trees supporting the first and second alternative topologies,
299 based on the rationale that under ILS the first and second alternative gene tree topologies should
300 be supported by an equal number of gene trees (Sayyari and Mirarab 2018). We identified 11 out
301 of 37 internal branches (30%) for which the number of gene trees supporting the two alternative
302 topologies were not significantly different (colored branches in **Fig. 1**). At these 11 internal
303 branches, ILS alone can thus explain gene tree heterogeneity, while asymmetries at the other 26
304 internal branches may need to invoke other processes.

305 **Contributions of Introgression to Gene Tree Heterogeneity**

306 Given that gene tree heterogeneity at many branches could not be explained by ILS alone, we set
307 out to infer footprints of introgression across wheatears. To this end, we first applied the approach
308 based on D-statistics (Durand et al. 2011) implemented in Dsuite, using > 58 million biallelic SNPs.
309 This approach estimates D and f4 statistics across all possible combinations of trios in wheatears
310 and then performs an f-branch test to assign gene flow to specific internal branches. The f-branch
311 test suggested multiple events of introgression (**Fig. 3**), namely between: (i) *O. halophila* and the
312 ancestor of *O. lugens lugens* and *O. warriae*, (ii) *O. xanthoprymna* and the ancestor of the *lugens*
313 complex, (iii) *O. leucopyga* and the ancestor of the *O. lugubris/lugentoides* clade, (iv) *O. picata*
314 *capistrata* and the ancestor of *O. picata picata* and *O. albonigra*, and (v) *O. melanoleuca* and *O.*
315 *pleschanka*.

316 Finally, we corroborated the evidence for introgression in the *hispanica, lugens,* and *picata*
317 complexes with multi-species coalescent network analyses in phyloNet, allowing for 0-5
318 introgression events. According to the Bayesian Information Criterion (BIC), models involving
319 reticulation events better fit the data than strictly bifurcating trees in all three complexes (**Tab.**

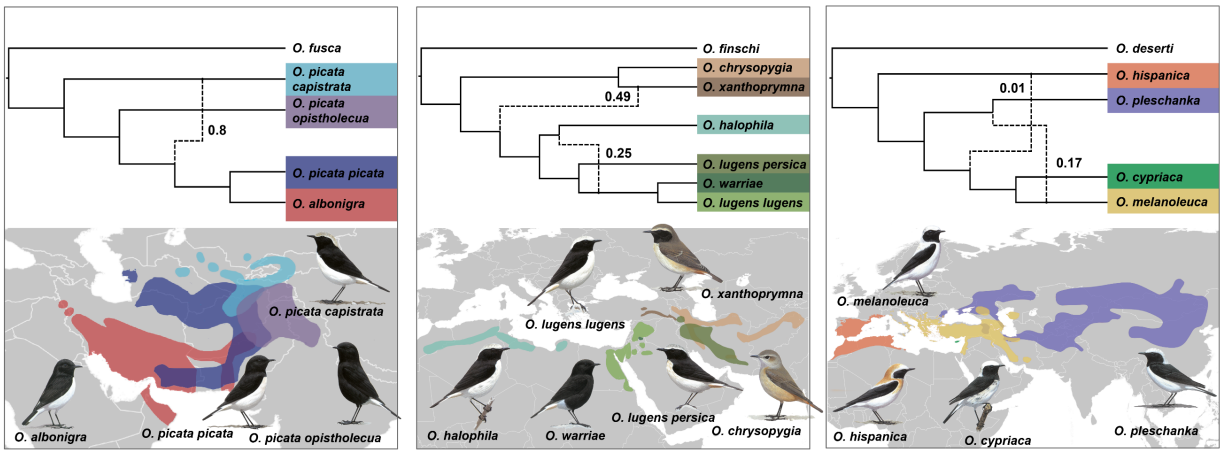

Figure 4 | Phylogenomic networks and distribution ranges for the *picata* (left), *lugens* (middle) and *hispanica* (right) complexes. Phylogenomic networks were estimated under the maximum pseudolikelihood approach implemented in phyloNet. Numbers on the edges indicate the inheritance probabilities, which correspond to the proportion of gene trees supporting the reticulate relationship. Drawings courtesy of Chris Rose (www.chrisrose-artist.co.uk) with permission from Bloomsbury Publishing Plc. Distribution ranges modified from BirdLife International and the Handbook of the Birds of the World (2016).

320 **S3**). In the *lugens* complex, two introgression events were detected: between *O. xanthoprymna*
321 and the ancestor of *O. lugens* (γ=49%), and between *O. halophila* and the *O. lugens lugens-O.*
322 *warriae* ancestor (γ=25%) (**Fig. 4**). One introgression event was detected in the *picata* complex,
323 between *O. picata capistrata* and the ancestor of *O. picata picata* and *O. albonigra* (γ=8%) (**Fig. 4**).
324 In the *hispanica* complex, the highest-scoring network involved two introgression edges: one
325 between *O. melanoleuca* and *O. pleschanka* (γ=17%), and one between *O. hispanica* and the *O.*
326 *cypriaca-melanoeuca* ancestor (γ=1%) (**Fig. 4**).

327 Discussion

328 The present study provides first genomic insights into the speciation history of open-habitat chats
329 and into the processes involved in shaping gene tree heterogeneity that may also underpin the
330 high incidence of convergent evolution in this group of songbirds. Our analyses reveal
331 unambiguous species relationships despite considerable gene tree heterogeneity, including
332 several mito-nuclear discordances that result from a combination of ILS and introgression. These
333 relationships reconstructed from genomic data provide the strongest evidence yet for abundant
334 convergent evolution in open-habitat chats, exemplified for three phenotypes in **Fig. 1**.
335 We first discuss how mito-nuclear discordances and incidences of introgression together
336 with known histories of hybridization and biogeography mold into a comprehensive picture of
337 open-habitat chat evolution. We close by concluding based on the indirect evidence presented
338 here that convergent evolution in open habitat chats likely involved a combination of ILS,
339 introgression and novel mutations in independent lineages. Together, our results paint a picture
340 of genomic and phenotypic evolution that is in part marked by the sharing of ancestral variation
341 and an exchange of genetic variation between species. Our study therefore contributes to the
342 increasing body of evidence that phenotypic and species evolution not only proceed from novel
343 mutations but abundantly reuse genetic variation present in ancestral and related species
344 (Marques et al. 2019b; Meier et al. 2018; Seehausen et al. 2014).

345 Mito-nuclear discordances, patterns of introgression, hybridization history, and 346 biography mold into a coherent picture of complex open-habitat chat evolution

347 The species relationships inferred from nuclear genomic data were in good agreement with
348 previous phylogenies based predominantly on single mitochondrial markers (Aliabadian et al.
349 2012; Schweizer and Shirihai 2013) and thereby confirmed the biogeographic history of open-
350 habitat chats (Alaei Kakhki et al. 2016). Still, we recovered several species relationships
351 discordant between the nuclear genome and the mitogenome (Toews and Brelsford 2012). In the
352 light of (i) the histories of introgression also uncovered here, (ii) the previously known
353 hybridization history deduced from observed instances of hybridization, and (iii) the here

354 confirmed biogeography, most of these mito-nuclear discordances can be well embedded in a
355 coherent history of open-habitat evolution.

356 The close nuclear relationship of *O. albonigra* with the nominate subspecies *O. p. picata* is in
357 stark contrast with the mitochondrial divergence of *O. albonigra* with all *O. picata* subspecies
358 about 0.5 mya (**Fig. 4a**). However, as an exception for wheatears, even from a perspective of
359 plumage coloration, the nuclear species tree implies a more parsimonious history of phenotypic
360 evolution, as *O. albonigra* and *O. p. picata* display almost identical plumages. The high
361 mitochondrial similarity of all subspecies currently treated under *O. picata* according to Panov
362 (2005) may be a result of introgressive hybridization. Indeed, the high abundance of admixed
363 phenotypes in zones of contact between the members of this species complex (Panov 2005)
364 suggests a high incidence of hybridization. Different from the *hispanica* complex, where taxa meet
365 in restricted zones, lineages of the *picata* complex all mold together in a relatively large area in
366 southern Central Asia, and their degree of reproductive isolation is largely unknown. Further
367 population genomic insights are required from the *picata* complex to obtain detailed insights into
368 its history of hybridization and phenotypic evolution.

369 The evolution of the *lugens* complex was marked by two incidences of introgression that
370 likely underpin the mito-nuclear discordance observed in this complex (**Fig. 4b**). Introgression
371 occurred between *O. xanthoprymna* and the *O. lugens* ancestor and between north-African *O.*
372 *halophila* and the middle eastern *O. l. lugens-O. warriae* ancestor. Both incidences of introgression
373 make sense in the light of biogeography, as they occurred between geographically neighboring
374 taxa (**Fig. 4b**). Together they can explain the close mitochondrial relationship of *O. l. persica* with
375 *O. xanthoprymna* and *O. chrysopygia*: *O. xanthoprymna* mitochondria were introduced into the *O.*
376 *lugens* ancestor by hybridization and may at first have segregated in the *O. lugens* lineage but then
377 have been lost in *O. halophila.* Mitochondrial replacement with *O. halophila* variation upon genetic
378 exchange of the latter taxon with the *O. l. lugens-O. warriae* ancestor would have left *O. l. persica*
379 the only taxon with a *O. xanthoprymna*-like mitogenome. Importantly, our results shed first
380 genomic light on the divergence of Basalt Wheatear (*O. warriae*), a species with a very restricted
381 range that is interesting from the perspective of phenotypic evolution: this species turns out to be
382 highly similar to *O. l. lugens* at the genomic level, which contrasts with its marked phenotypic
383 divergence (**Fig. 4b**). This result is similar to the situation observed, for instance, in Hooded and
384 Carrion Crows (*Corvus cornix* and *C. corone*, respectively) (Poelstra et al. 2014) and opens
385 interesting questions on the evolutionary history of this taxon's coloration.

386 Finally, in the *hispanica* complex, the incomplete sorting of mitochondrial variation was
387 previously well documented (Alaei Kakhki et al. 2018; Randler et al. 2012), and footprints of
388 introgression came as no surprise: The complex is characterized by pervasive hybridization of *O.*
389 *melanoleuca* with *O. pleschanka* in several geographic regions (Haffer 1977; Panov 1992) and

population genomic analyses suggest rates of introgression of up to almost 20% between these species (Schweizer et al. 2019a). Research is underway to uncover the detailed histories of hybridization in this Eurasian wheatear complex.

The thus far discussed mito-nuclear discordances were all accompanied with high levels of gene tree heterogeneity (most within the phylogenetic anomaly zone). However, most of these cases were not explained by ILS alone but went along with footprints of introgression. Still, part of the observed mito-nuclear discordances might well be a consequence of ILS. In the *picata* complex, for instance, lineage divergence occurred in rapid succession (**Fig. 1**), and ILS might well be an alternative explanation for the mitochondrial divergence of the *O. albonigra* mitogenome. In addition, in the clade including *O. heuglinii* and the very widespread *O. isabellina*, species split in fast succession and the high levels of ILS likely explain the observed mito-nuclear discordance.

Taken together, our results demonstrate that the speciation history of open-habitat chats is similarly complex as their phenotypic evolution. Multiple events of introgression at both extant and ancestral time scales, along with abundant ILS, contributed to reticulate evolution and thus a mosaic of genomic variation in several clades of wheatears. Our study thus adds to an increasing number of examples (Enciso-Romero et al. 2017; Han et al. 2017; Lamichhaney et al. 2018; Meier et al. 2017) highlighting that species diversification is often complex and rather than by a linear process is at least in part a network of interacting lineages (Marques et al. 2019b)

Diverse routes to convergent evolution in open-habitat chats

The reconstruction of relationships among open-habitat chats using genomic data has a deep impact on our understanding of phenotypic evolution in these songbirds: the species tree provides firm evidence for an extraordinary incidence of convergent evolution (**Fig. 1**). For numerous traits, including plumage coloration, sexual dimorphism, and migration behavior, not related species display more similar phenotypes than sister species (**Fig. 1**). Almost entirely black plumages, for instance, evolved in five clades (*O. picata opistholeuca*, *O. warriae*, *O. leucura*, female *M. monticola*, and juvenile *O. leucopyga*), and sexually monomorphic female-type plumage is found in another five clades (*O. chrysopygia*, *O. fusca*, the *O. melanura* clade, the *O. isabellina* clade, and in the sub-Saharan clade), to name just two out of many examples.

Furthermore, our results suggest (directly for introgression and ILS, indirectly for novel mutations) that convergent evolution in open-habitat chats is unlikely explained by a single process but may need to invoke all three processes (Hedrick 2013; Konečná et al. 2021; Montejo-Kovacevich et al. 2021; Natarajan et al. 2015; Pease et al. 2016), with the most likely processes depending on both demography and the phylogenetic scale.

For ILS to contribute to convergent evolution, species must diverge in fast succession and maintain critically high effective population sizes to pass on ancestral variation and maintain it in daughter lineages. In open-habitat chats, such fast radiations occurred predominantly at rather

426 recent time scales. The shortest split intervals are observed (in increasing order) in the *picata*,
427 *hispanica*, and *lugens* complexes (**Fig. 1**). However, convergent evolution of species in the *lugens*
428 complex and of the *picata* complex is only found with other clades but not within the complexes.
429 Given that the levels of ILS at the root of the *lugens* complex are restricted, ILS is unlikely to have
430 contributed to convergent evolution with other clades of wheatears sporting, for instance, similar
431 plumages (see for instance the aforementioned example including *O. warriae*). Convergent
432 evolution is, however, observed for back and neck-side coloration in the *hispanica* complex
433 (Schweizer et al. 2019a), and could be explained by ILS of ancestral variation.

434 Likewise, introgression would need to have happened between taxa with similar phenotype
435 to explain convergent evolution. Our analyses indeed uncovered several instances of in part
436 substantial introgression (**Fig. 3**, **Fig. 4**). However, despite suggesting that introgression upon
437 hybridization provided the opportunity to exchange phenotypes between species, none of the
438 inferred introgression events can be tied to concrete examples of convergent evolution. This
439 raises the question, whether the methods applied here are underpowered to infer footprints of
440 introgression relevant to phenotypic evolution of open-habitat chats, or, indeed, introgression
441 played a limited role in these songbirds' phenotypic evolution.

442 Finally, we may need to invoke novel mutations to explain at least part of the observed
443 convergent evolution, because phenotypic similarities are found between rather divergent
444 species and inferred instances of high ILS and introgression cannot easily explain them. Many if
445 not most phenotypic similarities in open-habitat chats are found in the rather distant major
446 phylogenetic clades that diverged around 5 mya (for instance the examples provided at the entry
447 of the discussion). The time tree suggests that the relevant split events did not occur within short
448 evolutionary time scales. Accordingly, levels of ILS are rather low for at least one of the relevant
449 nodes (**Fig. 1**). Although gene tree heterogeneity was non-negligible for the larger of the two
450 major wheatear clades, gene trees were mostly concordant for the root nodes of the wheatear
451 clade including the *hispanica* complex and the *O. oenanthe* and *O. isabellina* clades (**Fig. 1**).
452 Moreover, the phenotypically similar species occur in geographically well separated ranges and
453 introgression between them is thus rather unexpected. In conclusion, unless the approaches used
454 here to detect the ILS and introgression are underpowered, the indirect evidence provided by our
455 results suggests that many incidences of convergent evolution at such time scale may have
456 involved independent novel mutations.

457 **Conclusion**

458 In the present study we set out to probe gene tree variation for footprints of ILS and introgression
459 with the goal of understanding how ILS and introgression may have contributed to convergent
460 evolution in open-habitat chats. Our results reveal a complex speciation history and provide
461 conclusive evidence for abundant convergent evolutionin open-habitat chats. While we cannot

462 conclude on the involvement of specific processes in the evolution of specific convergent
463 evolution, the indirect evidence gained from the structure of the species tree and inferred levels
464 of ILS and introgression suggest that convergent evolution in open-habitat chats likely occurred
465 via all three possible processes, namely ILS, introgression, and novel mutations. Thereby, our
466 results contribute to a growing body of evidence that evolution makes use and re-use of all
467 resources it has at hand, including both standing (ancestral or heterospecific) as well as novel
468 genetic variation.

469 Finally, the approach applied here based predominantly on a characterization of gene tree
470 heterogeneity outlines an avenue to probe the processes governing convergent evolution in a
471 wide range of systems. Even though the evidence for the involvement of these processes is
472 indirect, ultimately, at a comparative scale this evidence may provide valuable insights into the
473 relative contributions of ILS, introgression, and novel mutations to convergent evolution.

474 Material and Methods

475 Taxon sampling, DNA extraction, and whole-genome resequencing

476 Aiming for complete taxon sampling, we sequenced the genomes of 50 open-habitat chat taxa from
477 a total of 44 species from the genera *Oenanthe*, *Campicoloides, Emarginata*, *Myrmecocichla*,
478 *Pinarochroa*, and *Thamnolaea* (**Fig. 2**; **Tab. S1**). This sampling included all but three species (*E.*
479 *tractrac*, *M. collaris*, *T. coronata*) of the 47 currently recognized open-habitat chat species (Gill et
480 al. 2020). A genome sequence of *Saxicola maurus* (European Nucleotide Archive accession
481 number: ERR2560200-ERR2560209), a species of open-habitat chats' sister lineage (Sangster et
482 al. 2010; Zuccon and Ericson 2010), was included as an outgroup to root the open-habitat chat
483 species tree. We followed the taxonomy of the IOC World Bird List (v12.1) (Gill et al. 2020) except
484 for the *picata* complex, where we treat subspecies *picata, capistrata* and *opistholeuca* separately,
485 following Panov (2005).

486 We extracted DNA from blood stored in ≥96% ethanol or Queen's Lysis buffer or tissues
487 stored in 96% ethanol for taxa for which fresh material was available, or from toepads or dried
488 skin from skin-preparation sutures for taxa for which only museum samples were available (**Tab.**
489 **S1**). From blood and tissue samples DNA was extracted using the DNeasy Blood and Tissue Kit
490 (Qiagen) or the MagAttract HMW DNA kit (Qiagen) following the manufacturer's protocol with
491 exception of an adapted digestion of blood samples as reported in Lutgen et al (Lutgen et al. 2020).
492 DNA from toepads and dried skin was extracted using the QIAamp DNA Micro Kit (Qiagen) with
493 an adapted digestion protocol that ensures high quantities of DNA
494 (dx.doi.org/10.17504/protocols.io.dm6gpwrdplzp/1). DNA concentrations were quantified on a
495 Qubit fluorometer (dsDNA BR assay, Thermo Fisher Scientific) and DNA integrity was evaluated
496 on a TapeStation (MANUFACTURER, KIT). We prepared sequencing libraries using the ThruPLEX

497 DNA-Seq Kit (Takara), the Illumina DNA Prep Kit, the Illumina DNA PCR-free Kit, or the Chromium
498 Genome Library kit (10X Genomics) for intact DNA, or for fragmented DNA with the ACCEL-NGS
499 1S DNA Library Prep Kit (Swift Biosciences) (**Tab. S1**). All libraries were sequenced (150 bp
500 paired-end) on Illumina NovaSeq6000 instruments with a target coverage of ca. 15x.

501 Data preparation

502 *Adapter trimming and mapping of resequencing data*

503 Prior to further analysis, for all but the linked-read sequencing data, we trimmed adapters and
504 merged overlapping paired-end reads using fastp 0.20.0 (Chen et al. 2018). For linked-read
505 sequences, we trimmed the first 22 bp on the R1 read to eliminate the 10X indexes. We then
506 mapped the reads to the reference genome assembly of *Oenanthe melanoleuca* (Peona et al. in
507 prep.) using BWA 0.7.17 (Li 2013) and marked duplications with PicardTools 2.9.1
508 (http://broadinstitute.github.io/picard). After excluding duplicates, the average sequencing
509 coverage per individual ranged from 4.6x to 40.6x (mean and median 12.2, standard deviation
510 6.20) (**Tab. S1**).

511 *Base quality score recalibration (BQSR), SNP calling, and SNP genotyping*

512 Data preparation followed the GATK 4.1.4.1 (McKenna et al. 2010) best practices pipeline. First,
513 to prepare a list of high-confidence SNPs for BQSR, we ran HaplotypeCaller to generate gvcf files
514 for each sample and then merged gvcf files of all samples with CombineGVCFs before genotyping
515 SNPs using GenotypeGVCFs. To retain only high-confidence SNPs in the SNP-exclude set for BQSR,
516 we retained only SNPs that fulfilled the following criteria: mapping quality > 40, Fisher strand (FS)
517 phred-scaled p-value < 60, SNP quality score > 20, mapping quality rank sum value > -12.5, read
518 pos rank-sum test value > -8.0 and quality by depth > 2. We retained only biallelic SNPs with at
519 least one homozygous reference and one homozygous alternative genotype or with at least three
520 observations of reference and alternative alleles. We excluded the resulting set of SNPs from BQSR
521 in GATK. Following BQSR, we ran HaplotypeCaller on base-score-recalibrated bam files. The
522 resulting gvcf files of all samples where merged (CombineGVCFs) and variant and invariant sites
523 genotyped using the 'include-non-variant-sites' flag in GenotypeGVCFs. For all subsequent
524 analyses we based genotypes on genotype likelihoods. This resulted in 871,428,254 unfiltered
525 sites when the outgroup was included and 872,152,150 unfiltered sites without the outgroup.

526 In phylogenomic data sets, which are based on mapping of resequencing data to a
527 reference genome, data of species more divergent from the reference genome may risk mapping
528 at a lower percentage. To check for such mapping-related biases in our dataset, we estimated the
529 average number of nucleotide differences (d_{XY}) between *Oenanthe melanoleuca* (reference
530 genome) and all other species using pixy 0.95.02 (Korunes and Samuk 2021). We then estimated

531 the mapping percentage for all species using SAMtools (Li et al. 2009) and tested whether there
532 was a correlation between d_{XY} and mapping success.

533 *Data filtering*

534 Before data analysis, we removed all repeat regions from the multi-sample VCF file using the
535 repeat mask reported in Peona et al. (in prep.). Then we used BCFtools 1.11 (Li 2011) to remove
536 indels, sites close to indels (up to 10 bp) and all the sites at which exclusively alternative alleles
537 were called. For analyses requiring variant sites only, we removed all SNPs with more than 20%
538 missing data and all invariant sites using BCFtools and retained only SNPs with a minimum read
539 depth of five. To ensure linkage-disequilibrium (LD) among SNPs, we LD-pruned SNPs in VCFtools
540 0.1.16 (Danecek et al. 2011) such as to only retain SNPs with a minimum distance of 1 kb between
541 them. This physical distance is expected to remove most LD between SNPs, as e.g. in flycatchers
542 LD breaks down in most genomic regions after 1 kb (Ellegren et al. 2012). After this filtering, we
543 genotyped based on genotype likelihoods and retained 994,150 multiallelic SNPs. In addition, for
544 analyses that require biallelic SNPs exclusively, we removed all multiallelic SNPs from the VCF file
545 after the above filtering, using BCFtools.

546 For phylogenomic analyses requiring sequence data including both variant and invariant
547 sites, we followed two strategies. First, we defined 10 kb non-overlapping windows across the
548 genome. Henceforth, we refer to the windowed data as "loci" and to phylogenetic trees inferred
549 therefrom as "gene trees". Second, we inferred benchmarking universal single-copy orthologs,
550 BUSCO, using BUSCO 5.0.0 (Simão et al. 2015). Similar to ultraconserved elements, UCE (Faircloth
551 et al. 2012), BUSCO feature a high degree of conservation and moreover are present in single
552 copies, circumventing issues with paralogs in phylogenomic reconstructions (Roy 2009). BUSCO
553 are readily identified in whole-genome resequencing data sets, not requiring genome alignments,
554 and are increasingly deployed for phylogenomic reconstructions (Kallal et al. 2021; Van Damme
555 et al. 2022).

556 To make sure that the adopted filtering strategy did not affect our results, we generated
557 four sets of fasta alignments using different filter settings for minimum read depth (DP), minimum
558 percentage of the window covered by data (PW), and missing data per site (MD) for both the 10
559 kb loci and the BUSCO data set: (i) DP=1, PW=50%, MD=15%, (ii) DP=5, PW=50%, MD=15%, (iii)
560 DP=1, PW=50%, MD=5%, and (iv) DP=1, PW=80%, MD=10% (**Tab. S2**). These four filtering
561 strategies yielded the same species tree and concatenated tree for 10 kb loci as well as for BUSCO.
562 For these analyses, we therefore exclusively report the results based on the most stringent
563 filtering on read depth (ii, DP=5, PW=50%, MD=15%) (**Tab. S2**). For gene tree heterogeneity
564 analyses, on the other hand, we aimed to include the broadest representation of the genome and
565 to this end retained all loci (N=29,730) that fulfilled less stringent filtering criteria (i, DP=1,
566 PW=50%, MD=15%) (**Tab. S2**).

567 Finally, for analyses making assumptions on intra- and inter-locus recombination (such as
568 species tree reconstructions) we made sure to include only loci with no intra-locus but free inter-
569 locus recombination **(Tab. S2**). To this end, we excluded all loci with recombination signals (P ≤
570 0.05) as inferred from the pairwise homoplasy index Phi (Φw) estimated in PhiPack 1.1 program
571 (Bruen et al. 2006). The criterion P ≤ 0.05 does not account for multiple testing, but we preferred
572 to conservatively exclude loci with evidence for intra-locus recombination. To possibly retain only
573 loci among which free recombination occurs, we ensured a minimum distance of 10 kb by
574 including no two consecutive loci. At this distance, no LD occurs in flycatchers (Ellegren et al.
575 2012).

576 *Inference of Benchmarking Universal Single-Copy Ortholog (BUSCO) sequences*
577 Phylogenomic analyses based on the mapping of resequencing data to a reference genome,
578 especially when including species well diverged from the latter, may be affected by several biases.
579 For species more divergent from the reference genome, data from faster evolving genomic regions
580 (i) risks not being mapped, if these regions are too diverged from the reference sequence, or (ii)
581 may map to paralogs, if the species experienced different duplication histories (Chakrabarty et al.
582 2017; Fitz-Gibbon et al. 2017). These biases are expected to be least important in slowly evolving
583 regions of the genome, especially in BUSCO, that are conserved and by definition present in single
584 copies in most species. To minimize mapping-related biases in our phylogenomic reconstructions,
585 especially on rooting and placements of the most divergent species, we therefore extracted the
586 intervals in which avian BUSCO (aves_odb10) are situated in our reference genome using BUSCO
587 5.0.0 (Simão et al. 2015).

588 **Phylogenomic reconstructions and multispecies coalescent analyses**
589 *BUSCO-based rooting of the open-habitat chat species tree*
590 First, to establish the root within open-habitat chats, we applied both concatenation and
591 multispecies coalescent-based methods on BUSCO sequences, including the outgroup. First, we
592 used all BUSCO (N=7,335) to estimate the maximum likelihood tree in IQ-TREE 2.1.2 (Minh et al.
593 2020b) based on the concatenated BUSCO, using with one partition for each BUSCO and a
594 GTR+I+G substitution model for all partitions (Abadi et al. 2019). One thousand bootstrap
595 replicates were run using the ultrafast bootstrap approximation (Hoang et al. 2018). Second, we
596 estimated the species tree under the multispecies coalescent using ASTRAL-III (Zhang et al. 2018)
597 based on BUSCO without recombination signals and free inter-locus recombination (N=2,091). To
598 this end, we inferred BUSCO' gene trees in IQ-TREE 2.1.2 using a GTR+I+G substitution model and
599 one thousand ultrafast bootstrap approximations. To ensure that species tree inferences were not
600 affected by inaccurately estimated gene trees (Zhang et al. 2018), we collapsed branches with
601 bootstrap support inferior to 80% using Newick Utilities 1.6 (Junier and Zdobnov 2010).

602 Reconstructing the species tree by including all BUSCO not considering intra- and inter-locus
603 recombination (N=7,335) did not affect the result.

604 *Phylogenomic and multispecies coalescent analyses based on full evidence*
605 To reconstruct the concatenated tree and species tree based on full evidence data, that is, data
606 from the maximal possible fraction of the genome, and to study gene tree heterogeneity along the
607 genome, we excluded the *Saxicola* outgroup. Instead, we rooted the trees with the clade that is the
608 outgroup to all other open-habitat chats (sub-Saharan clade, **Fig. S1**). Excluding *Saxicola* ensured
609 that analyses were not biased by mapping issues caused by this outgroup's divergence.
610 To estimate the concatenated tree using maximum likelihood in IQ-TREE 2.1.2 we used all
611 loci with a GTR+I+G substitution model and 1,000 ultrafast bootstrap approximations. To
612 estimate the species tree under the multispecies coalescent using ASTRAL-III, we at first
613 estimated maximum likelihood gene trees using IQ-TREE 2.1.2 with a GTR+I+G substitution model
614 and one thousand ultrafast bootstrap approximations. Based on these gene trees (pruned for
615 within-locus recombination and assuring free recombination between loci), we inferred the
616 species tree using ASTRAL-III. Because ASTRAL relies on accurately estimated gene trees, we
617 collapsed branches with bootstrap support inferior to 80% using Newick Utilities 1.6.
618 To find regions of the species tree that represent "anomaly zones" where the frequency of
619 one of the alternative quartets is higher than that of the topology in agreement the species tree,
620 we estimated local quartet supports for the main topology and its two alternatives in ASTRAL-III
621 (Degnan and Rosenberg 2006). We used the anomaly_finder.py script to search for anomaly zones
622 in our species tree (Linkem et al. 2016). To test if the gene tree discordance could be explained by
623 polytomies instead of bifurcating nodes, we carried out a quartet-based polytomy test as
624 implemented in ASTRAL-III.
625 To see whether the SNP-based species tree could confirm the sequence-based species tree,
626 we used the unlinked multiallelic SNPs to the multispecies coalescent model implemented in
627 SVDQuartets (Chifman and Kubatko 2014) in PAUP* 4 (Swofford 2003). We ran this with 1000
628 bootstrap replicates and summarized the result in a 50% majority-rule consensus tree.

629 *Phylogenetic relationships of mitogenomes*
630 We were interested in whether previously inferred relationships based predominantly on single
631 mitochondrial genes (Alaei Kakhki et al. 2016; Aliabadian et al. 2012; Schweizer and Shirihai
632 2013) were supported by full mitogenomes and in how the mitogenomic relationships compare
633 to the ones inferred from nuclear loci. To this end, we extracted and assembled mitochondrial
634 genomes from the genomic data of all open-habitat chats using MitoFinder 1.2 (Allio et al. 2020).
635 We used the published Isabelline Wheatear (*Oenanthe isabellina*) mitochondrial genome as a
636 reference (Genbank accession number: NC_040290.1) and annotated the mitochondrial genome

637 using the annotation pipeline integrated in MitoFinder. Finally, we aligned the 13 mitochondrial
638 protein coding gene sequences using the automatic alignment strategy in MAFFT 7.471 (Katoh
639 and Standley 2013). We checked the alignments in AliView 1.26 (Larsson 2014) and removed stop
640 codons within the coding sequences or indels for downstream analyses. We determined the best
641 partition scheme using the Akaike information criterion (AIC) implemented in PartitionFinder
642 2.1.1 (Lanfear et al. 2017) and used the GTR+G+I model for all partitions. Then we constructed
643 the maximum-likelihood tree from the concatenated supermatrix of all 13 genes in IQ-TREE 2.1.2
644 using the ultrafast bootstrap approximations with 1,000 replicates.

645 **Dating analyses**

646 Beside species' relationships we were interested in estimating the divergence time in open-
647 habitat chats. Because there are no appropriate fossils for calibration, we first ran BEAST 2.6.6
648 (Bouckaert et al. 2019) for 13 mitochondrial protein coding genes to estimate a time-calibrated
649 mitochondrial phylogeny. We included the mitochondrial genome sequence of *Saxicola maurus*
650 (GenBank accession number: MN356403.1) as an outgroup in these analyses. Substitution models
651 were inferred during the MCMS analyses with bModelTest (Bouckaert and Drummond 2017)
652 implemented as a package in BEAST 2.6.6. Published substitution rates for each mitochondrial
653 gene (Lerner et al. 2011) were implemented as means of the clock rates in real space of lognormal
654 distribution with standard deviations of 0.005. We defined a Yule speciation process for the tree
655 prior and an uncorrelated lognormal relaxed clock model. Three independent MCMC chains were
656 run for 50 million generations, each with sampling every 5,000 generations. Effective sample sizes
657 for all parameters and appropriate numbers of burn-in generations were checked with Tracer 1.5
658 (Rambaut and Drummond 2009). The three independent runs were combined using LogCombiner
659 2.6.6 (Bouckaert et al. 2019). We used TreeAnnotator 2.6.6 (Bouckaert et al. 2019) to calculate a
660 maximum clade credibility tree and the 95% highest posterior density (HPD) distributions of each
661 estimated node.

662 We then used the divergence time of the sub-Saharan clade from wheatears estimated
663 from mitochondrial data as time constraint in dating analyses based on nuclear data using
664 RelTime-ML implemented in MEGA 11 (Tamura et al. 2021). For this analysis, we provided the
665 topology with branch length estimated in IQtree2 based on concatenated BUSCO data retained
666 after the most stringent filtering (ii, DP=5, PW=50%, MD=15%), along with high-confidence
667 BUSCO alignments. The latter consisted of BUSCO data filtered for DP=5, MD=5% and length of
668 each BUSCO alignments longer than 1kb. We used the same filtering to get the 10 kb non-
669 overlapping windows across the genome and used the concatenated tree retained after most
670 stringent filtering (ii, DP=5, PW=50%, MD=15%) to repeat the analyses based on loci across the
671 genome. To ensure that the differences in divergence times between mitochondrial and nuclear

672 data were not due to the different dating approaches, we re-estimated the mitochondrial
673 divergence times in RelTime-ML using the same approach as for the nuclear datasets.

674 Inference of gene tree variation, ILS, and introgression

675 *Inference of the levels of gene tree variation*

676 To investigate gene tree heterogeneity across the genome, we used gene trees inferred from less
677 stringent filtering criteria (i, DP=1, PW=50%, MD=15%) as described above. To infer how many
678 gene trees reflect the species tree topology, we used the script 'findCommonTrees.py' (Edelman
679 et al. 2019). To characterize the levels of gene tree heterogeneity across open-habitat chats, we
680 compared the gene trees to the species tree. Specifically, we estimated "internode certainty all"
681 (ICA) and the "gene concordance factor" (gCF). ICA quantifies the amount of gene tree
682 heterogeneity for each internode of the species tree by calculating the number of all most
683 prevalent conflicting bipartitions. It takes values ranging from -1 to 1, with values around zero
684 indicating strong conflict; values towards 1 indicate robust concordance of gene trees with the
685 species tree in the bipartition of interest; and negative values indicate discordance between the
686 bipartition of interest and one or more bipartitions with a higher frequency (Salichos et al. 2014).
687 While ICA thus represents the degree of conflict on each node of a species tree, gCF better reflects
688 the gene tree heterogeneity around each branch, and is the percentage of gene trees supporting
689 the two alternative topologies for each branch (Minh et al. 2020a). We estimated ICA and gCF with
690 PhyParts 0.0.1 (Smith et al. 2015) and IQ-TREE 2.1.2 respectively.

691 *Tests of an ILS model*

692 Next, we were interested in understanding whether ILS can sufficiently explain the level of gene
693 tree heterogeneity observed at the level of the whole species tree. To this end, we applied the Tree
694 Incongruence Checking in R (TICR) test (Stenz et al. 2015) implemented in the Phylolm R package.
695 This test evaluates whether the multispecies coalescent adequately explains gene tree
696 heterogeneity across the species tree with no hybridization edges. TICR requires posterior
697 distributions of gene tree topologies inferred through Bayesian inference of gene trees. Therefore,
698 we first estimated posterior distributions of individual gene trees with MrBayes 3.2.7 (Ronquist
699 et al. 2012). MrBayes analyses ran using three independent runs of 20 million generations each,
700 sampling every 20,000th generation using a GTR+I+G model. We estimated the length of burn-in
701 using Tracer 1.5 (Rambaut and Drummond 2009) to ensure that our sampling of the posterior
702 distribution had reached sufficient effective sample sizes (ESS > 200) for parameter estimation.
703 We then ran BUCKy (Ané et al. 2007; Larget et al. 2010) using the posterior distribution of gene
704 trees after discarding 25% as burn-in to estimate the concordance factors (CFs) for the three
705 possible splits of all quartets. The inferred CF values were then tested against those expected
706 under a coalescent model that takes ILS but not hybridization into account (chi-squared test).

707 We then tested for each branch in the species tree whether the gene tree heterogeneity
708 reflected in gCF can be sufficiently explained by a model incorporating ILS alone. Under ILS alone
709 – assuming sorting of variation occurs by random genetic drift – proportions of alternative gene
710 trees for a rooted triplet are expected to be approximately equal (Hibbins and Hahn 2022; Sayyari
711 and Mirarab 2018; Sayyari et al. 2018), and the concordant tree topology (the topology in
712 agreement with the species tree) should be at least as frequent as the two discordant topologies
713 (Hibbins and Hahn 2022; Sayyari et al. 2018). In contrast, introgression between non-sister taxa
714 results in asymmetric proportions of gene trees in the rooted triplet (Durand et al. 2012; Green et
715 al. 2010). Therefore, we performed a chi-square tests comparing the number of gene trees
716 supporting the two discordant topologies. Under ILS, these two alternative topologies are
717 expected to be equally frequent among gene trees (He et al. 2020). For all these analyses we
718 accounted for uncertainty in gene tree topologies by collapsing branches with bootstrap support
719 <80%.

720 *Inferring footprints of introgression*

721 To infer footprints of introgression across the entire species tree, we estimated Patterson's D
722 (Durand et al. 2011) and related statistics in Dsuite (Malinsky et al. 2021) based on 58,963,109
723 biallelic SNPs. D and f4 statistics were estimated across all possible combinations of trios in our
724 38 wheatear taxa. We used Dtrios to calculate the sums of three different patterns (BABA, BBAA
725 and, ABBA) and D and f4-ratio statistics for all 8,437 possible trios. Dsuite uses the standard block-
726 jackknife procedure to assess the significance of the D statistic. Due to the large number of D-
727 statistics comparisons and difficulties disentangling false positives that may arise due to ancient
728 gene flow, we performed the f-branch test (fb) implemented in Dsuite to assign gene flow to
729 specific internal branches on the species tree. Then we visualized the output using Dsuite's
730 dtools.py script.

731 We then aimed to obtain further support for the footprints of introgression that were
732 suggested in *lugens, picata* and *hispanica* complex by the above approach based on the D-statistics.
733 To this end, for these three complexes, we estimated phylogenetic networks from maximum
734 likelihood trees generated from BUSCO using the pseudolikelihood (InferNetwork_MPL) (Yu and
735 Nakhleh 2015) and likelihood (CalGTProb) (Yu et al. 2014) approaches implemented in phyloNet
736 3.6.9 (Than et al. 2008). Due to the high computational demands, analyses were run for each of
737 the clades containing signals of introgression in earlier analyses separately, namely for the *lugens,*
738 *picata* and *hispanica* complexes. Furthermore, we only included BUSCO loci that had data
739 available for all taxa of the respective complex. Outgroup species for each complex were selected
740 based on the species tree. Analyses included 7,323 rooted gene trees for the *lugens* complex, 7,310
741 rooted gene trees for the *picata* complex, and 7,335 rooted gene trees for the *hispanica* complex.
742 For each complex, we allowed for one to five reticulation events, with the starting tree

743 corresponding to the species tree topology (-s), 0.9 bootstrap threshold for gene trees (-b) and
744 1,000 iterations (-x). To ensure convergence, the network searches were repeated 10 times. Then
745 we estimated the likelihood by fixing the topology of the focal clade for the species tree (without
746 any reticulation) and for each of the five networks (with different numbers of introgression edges)
747 and calculated their likelihood scores. We determined the optimal network by calculating the
748 Bayesian Information Criterion (BIC) from the maximum likelihood scores, the number of gene
749 trees, the number of branch length being estimated, plus the number of admixture edges in each
750 model (**Tab. S3**). We used the browser-based tree viewer IcyTree (Vaughan 2017) to visualize
751 the estimated networks.

752 Acknowledgements

753 We thank all the natural history museums and their staff who provided material for this study:
754 namely the American Museum of Natural History, New York; Natural History Museum, Tring; Field
755 Museum of Natural History, Chicago; Natural History Museum of Los Angeles County, Los Angeles;
756 Museum of Vertebrate Zoology, UC Berkeley; Natural History Museum, University of
757 Oslo; Naturhistoriska Riksmuseet, Stockholm; Texas A&M University Biodiversity Research and
758 Teaching Collections, Texas College Station; University of Washington Burke Museum;, Seattle,
759 Yale Peabody Museum; Zoological Museum, Natural History Museum of Denmark, Copenhagen;
760 Zoologisches Forschungsmuseum König, Bonn; and Martin Haase, Vogelwarte Hiddensee,
761 Universität Greifswald. Further samples were provided by José Luis Copete, and Marc Illa. We are
762 indebted to the sequencing facilities of NGI Sweden in Solna and to the NGS platform of the
763 University of Berne and their respective staff for their excellent services and to Marta Burri for
764 sequencing library preparations. Computations were performed at the High-Performance
765 Computing Cluster EVE, a joint effort of the Helmholtz Centre for Environmental Research (UFZ)
766 and the German Centre for Integrative Biodiversity Research (iDiv) Halle-Jena-Leipzig. We thank
767 the administration and support staff of EVE, Thomas Schnicke and Ben Langenberg (UFZ), and
768 Christian Krause (iDiv). We thank Chris Rose and Claire Weatherhead from Bloomsbury
769 Publishing Plc for their permission to use bird drawings in our figures. This research was
770 supported by a German Research Foundation (DFG) research grant (BU3456/3-1) to RB, the
771 National Research Fund (FNR), Luxembourg, grant number 14575729 to DL, and a Georg Foster
772 Research Stipend of the Alexander von Humboldt Foundation and a scholarship for female
773 researchers from Friedrich-Schiller-University Jena, both to NAK.

Author Contributions

RB and NAK designed the study. NAK, DL and MS performed data analysis with inputs from HSch and RB. RCKB, AS and HShi provided materials. MS designed the figures. NAK and RB wrote the manuscript with help from MS and HSch and inputs from all authors.

Data Availability

All sequencing data produced in the framework of this study are available on the European Nucleotide Archive (ENA) under accession number *XYZ (to be announced upon acceptance of the article)*.

References

Abadi S, Azouri D, Pupko T, Mayrose I. 2019. Model selection may not be a mandatory step for phylogeny reconstruction. *Nat Commun.*10(1):1-11.

Alaei Kakhki N, Aliabadian M, Förschler MI, Ghasempouri SM, Kiabi BH, Verde Arregoitia LD, Schweizer M. 2018. Phylogeography of the oenanthe hispanica–pleschanka–cypriaca complex (aves, muscicapidae: Saxicolinae): Diversification history of open-habitat specialists based on climate niche models, genetic data, and morphometric data. *Zoolog Syst Evol Res.* 56(3):408-427.

Alaei Kakhki N, Aliabadian M, Schweizer M. 2016. Out of africa: Biogeographic history of the open-habitat chats (aves, muscicapidae: Saxicolinae) across arid areas of the old world. *Zoologica Scripta* 45(3):237-251.

Aliabadian M, Kaboli M, Förschler MI, Nijman V, Chamani A, Tillier A, Prodon R, Pasquet E, Ericson PG, Zuccon D. 2012. Erratum to: Convergent evolution of morphological and ecological traits in the open-habitat chat complex (aves, muscicapidae: Saxicolinae). *Mol Phylogenet Evol.* 65(3):35-45.

Allio R, Schomaker-Bastos A, Romiguier J, Prosdocimi F, Nabholz B, Delsuc F. 2020. Mitofinder: Efficient automated large-scale extraction of mitogenomic data in target enrichment phylogenomics. *Mol Ecol Resour.* 20(4):892-905.

Ané C, Larget B, Baum DA, Smith SD, Rokas A. 2007. Bayesian estimation of concordance among gene trees. *Mol Biol Evol.* 24(2):412-426.

Arendt J, Reznick D. 2008. Convergence and parallelism reconsidered: What have we learned about the genetics of adaptation? *Trends Ecol Evol.* 23(1):26-32.

Barrett RD, Schluter D. 2008. Adaptation from standing genetic variation. *Trends Ecol Evol.* 23(1):38-44.

Besnard G, Muasya AM, Russier F, Roalson EH, Salamin N, Christin P-A. 2009. Phylogenomics of c4 photosynthesis in sedges (cyperaceae): Multiple appearances and genetic convergence. *Mol Biol Evol.* 26(8):1909-1919.

Bouckaert R, Vaughan TG, Barido-Sottani J, Duchêne S, Fourment M, Gavryushkina A, Heled J, Jones G, Kühnert D, De Maio N. 2019. Beast 2.5: An advanced software platform for bayesian evolutionary analysis. *PLoS Comput. Biol.* 15(4):e1006650.

812 Bouckaert RR, Drummond AJ. 2017. Bmodeltest: Bayesian phylogenetic site model averaging and
813 model comparison. *BMC Evol Biol.* 17(1):1-11.

814 Bruen TC, Philippe H, Bryant D. 2006. A simple and robust statistical test for detecting the
815 presence of recombination. *Genetics* 172(4):2665-2681.

816 Brusatte SL, O'Connor JK, Jarvis ED. 2015. The origin and diversification of birds. *Curr Biol.*
817 25(19):R888-R898.

818 Campagna L, Repenning M, Silveira LF, Fontana CS, Tubaro PL, Lovette IJ. 2017. Repeated
819 divergent selection on pigmentation genes in a rapid finch radiation. *Sci Adv.*
820 3(5):e1602404.

821 Chakrabarty P, Faircloth BC, Alda F, Ludt WB, Mcmahan CD, Near TJ, Dornburg A, Albert JS,
822 Arroyave J, Stiassny ML. 2017. Phylogenomic systematics of ostariophysan fishes:
823 Ultraconserved elements support the surprising non-monophyly of characiformes. *Syst*
824 *Biol.* 66(6):881-895.

825 Chen S, Zhou Y, Chen Y, Gu JJB. 2018. Fastp: An ultra-fast all-in-one fastq preprocessor.
826 34(17):i884-i890.

827 Chifman J, Kubatko L. 2014. Quartet inference from snp data under the coalescent model.
828 *Bioinformatics* 30(23):3317-3324.

829 Chou J, Gupta A, Yaduvanshi S, Davidson R, Nute M, Mirarab S, Warnow T. 2015. A comparative
830 study of svdquartets and other coalescent-based species tree estimation methods. *BMC*
831 *Genom.* 16(10):1-11.

832 Christin P-A, Salamin N, Savolainen V, Duvall MR, Besnard G. 2007. C4 photosynthesis evolved in
833 grasses via parallel adaptive genetic changes. *Curr Biol.* 17(14):1241-1247.

834 Colosimo PF, Hosemann KE, Balabhadra S, Villarreal G, Dickson M, Grimwood J, Schmutz J, Myers
835 RM, Schluter D, Kingsley DM. 2005. Widespread parallel evolution in sticklebacks by
836 repeated fixation of ectodysplasin alleles. *Science* 307(5717):1928-1933.

837 Cresko WA, Amores A, Wilson C, Murphy J, Currey M, Phillips P, Bell MA, Kimmel CB, Postlethwait
838 JH. 2004. Parallel genetic basis for repeated evolution of armor loss in alaskan threespine
839 stickleback populations. *PNAS*. 101(16):6050-6055.

840 Danecek P, Auton A, Abecasis G, Albers CA, Banks E, DePristo MA, Handsaker RE, Lunter G, Marth
841 GT, Sherry ST. 2011. The variant call format and vcftools. *Bioinformatics* 27(15):2156-
842 2158.

843 Degnan JH, Rosenberg NA. 2006. Discordance of species trees with their most likely gene trees.
844 *PLoS Genet*. 2(5):e68.

845 Doyle JJ. 1997. Trees within trees: Genes and species, molecules and morphology. *Syst Biol.*
846 46(3):537-553.

847 Durand EY, Patterson N, Reich D, Slatkin M. 2011. Testing for ancient admixture between closely
848 related populations. *Mol Biol Evol.* 28(8):2239-2252.

849 Durand S, Bouché N, Strand EP, Loudet O, Camilleri C. 2012. Rapid establishment of genetic
850 incompatibility through natural epigenetic variation. *Curr Biol.* 22(4):326-331.

851 Edelman NB, Frandsen PB, Miyagi M, Clavijo B, Davey J, Dikow RB, García-Accinelli G, Van
852 Belleghem SM, Patterson N, Neafsey DE. 2019. Genomic architecture and introgression
853 shape a butterfly radiation. *Science* 366(6465):594-599.

854 Ellegren H, Smeds L, Burri R, Olason PI, Backström N, Kawakami T, Künstner A, Mäkinen H,
855 Nadachowska-Brzyska K, Qvarnström A. 2012. The genomic landscape of species
856 divergence in ficedula flycatchers. *Nature* 491(7426):756-760.

857 Elmer KR, Meyer A. 2011. Adaptation in the age of ecological genomics: Insights from parallelism
858 and convergence. *Trends Ecol Evol.* 26(6):298-306.

859 Enciso-Romero J, Pardo-Díaz C, Martin SH, Arias CF, Linares M, McMillan WO, Jiggins CD, Salazar
860 C. 2017. Evolution of novel mimicry rings facilitated by adaptive introgression in tropical
861 butterflies. *Mol Ecol.* 26(19):5160-5172.

862 Eyre-Walker A, Keightley PD. 2007. The distribution of fitness effects of new mutations. *Nat Rev*
863 *Genet.* 8(8):610-618.

864 Faircloth BC, McCormack JE, Crawford NG, Harvey MG, Brumfield RT, Glenn TC. 2012.
865 Ultraconserved elements anchor thousands of genetic markers spanning multiple
866 evolutionary timescales. *Syst Biol.* 61(5):717-726.

867 Fitz-Gibbon S, Hipp AL, Pham KK, Manos PS, Sork VL. 2017. Phylogenomic inferences from
868 reference-mapped and de novo assembled short-read sequence data using radseq
869 sequencing of california white oaks (quercus section quercus). *Genome* 60(9):743-755.

870 Funk DJ, Omland KE. 2003. Species-level paraphyly and polyphyly: Frequency, causes, and
871 consequences, with insights from animal mitochondrial DNA. *Annu Rev Ecol Evol.*
872 34(1):397-423.

873 Genner MJ, Turner GF. 2012. Ancient hybridization and phenotypic novelty within lake malawi's
874 cichlid fish radiation. *Mol Biol Evol.* 29(1):195-206.

875 Gill F, Donsker D, Rasmussen P. 2020. Ioc world bird list (v10. 1). IOC World Bird List [consultado
876 el 26 de julio de 2020] DOI: https://doi org/1014344/IOC ML. 10.

877 Grant PR, Grant BR, Petren K. 2005. Hybridization in the recent past. *Am Nat.* 166(1):56-67.

878 Green RE, Krause J, Briggs AW, Maricic T, Stenzel U, Kircher M, Patterson N, Li H, Zhai W, Fritz MH-
879 Y. 2010. A draft sequence of the neandertal genome. *Science* 328(5979):710-722.

880 Gross JB, Borowsky R, Tabin CJ. 2009. A novel role for mc1r in the parallel evolution of
881 depigmentation in independent populations of the cavefish astyanax mexicanus. *PLoS*
882 *Genet.* 5(1):e1000326.

883 Haffer J. 1977. Secondary contact zones of birds in northern iran. *Bonn Zool Monogr.* 10:1-64.

884 Han F, Lamichhaney S, Grant BR, Grant PR, Andersson L, Webster MT. 2017. Gene flow, ancient
885 polymorphism, and ecological adaptation shape the genomic landscape of divergence
886 among darwin's finches. *Genome Res.* 27(6):1004-1015.

887 He C, Liang D, Zhang P. 2020. Asymmetric distribution of gene trees can arise under purifying
888 selection if differences in population size exist. *Mol Biol Evol.* 37(3):881-892.

889 Hedrick PW. 2013. Adaptive introgression in animals: Examples and comparison to new mutation
890 and standing variation as sources of adaptive variation. *Mol Ecol.* 22(18):4606-4618.

891 Heliconius Genome Consortium. 2012. Butterfly genome reveals promiscuous exchange of
892 mimicry adaptations among species. *Nature* 487:94-98.

893 Hermisson J, Pennings PS. 2005. Soft sweeps: Molecular population genetics of adaptation from
894 standing genetic variation. *Genetics* 169(4):2335-2352.

895 Hibbins MS, Hahn MW. 2022. Phylogenomic approaches to detecting and characterizing
896 introgression. *Genetics* 220(2):iyab173.

897 Hoang DT, Chernomor O, Von Haeseler A, Minh BQ, Vinh LS. 2018. Ufboot2: Improving the
898 ultrafast bootstrap approximation. *Mol Biol Evol.* 35(2):518-522.

899 Hoballah ME, Gübitz T, Stuurman J, Broger L, Barone M, Mandel T, Dell'Olivo A, Arnold M,
900 Kuhlemeier C. 2007. Single gene–mediated shift in pollinator attraction in petunia. *The*
901 *Plant Cell* 19(3):779-790.

902 Hobolth A, Dutheil JY, Hawks J, Schierup MH, Mailund T. 2011. Incomplete lineage sorting patterns
903 among human, chimpanzee, and orangutan suggest recent orangutan speciation and
904 widespread selection. *Genome Res.* 21(3):349-356.

905 Jarvis ED, Mirarab S, Aberer AJ, Li B, Houde P, Li C, Ho SY, Faircloth BC, Nabholz B, Howard JT.
906 2014. Whole-genome analyses resolve early branches in the tree of life of modern birds.
907 *Science* 346(6215):1320-1331.

908 Jones FC, Grabherr MG, Chan YF, Russell P, Mauceli E, Johnson J, Swofford R, Pirun M, Zody MC,
909 White S. 2012. The genomic basis of adaptive evolution in threespine sticklebacks. *Nature*
910 484(7392):55-61.

911 Junier T, Zdobnov EM. 2010. The newick utilities: High-throughput phylogenetic tree processing
912 in the unix shell. *Bioinformatics* 26(13):1669-1670.

913 Kallal RJ, Kulkarni SS, Dimitrov D, Benavides LR, Arnedo MA, Giribet G, Hormiga G. 2021.
914 Converging on the orb: Denser taxon sampling elucidates spider phylogeny and new
915 analytical methods support repeated evolution of the orb web. *Cladistics* 37(3):298-316.

916 Katoh K, Standley DM. 2013. Mafft multiple sequence alignment software version 7:
917 Improvements in performance and usability. *Mol Biol Evol.* 30(4):772-780.

918 Konečná V, Bray S, Vlček J, Bohutínská M, Požárová D, Choudhury RR, Bollmann-Giolai A, Flis P,
919 Salt DE, Parisod C. 2021. Parallel adaptation in autopolyploid arabidopsis arenosa is
920 dominated by repeated recruitment of shared alleles. *Nat Commun.* 12(1):1-13.

921 Korunes KL, Samuk K. 2021. Pixy: Unbiased estimation of nucleotide diversity and divergence in
922 the presence of missing data. *Mol Ecol Resour.* 21(4):1359-1368.

923 Kumar S, Stecher G, Li M, Knyaz C, Tamura K. 2018. Mega x: Molecular evolutionary genetics
924 analysis across computing platforms. *Mol Biol Evol.* 35(6):1547.

925 Lamers RP, Muthukrishnan G, Castoe TA, Tafur S, Cole AM, Parkinson CL. 2012. Phylogenetic
926 relationships among staphylococcus species and refinement of cluster groups based on
927 multilocus data. *BMC Evol Biol.* 12(1):1-15.

928 Lamichhaney S, Han F, Webster MT, Andersson L, Grant BR, Grant PR. 2018. Rapid hybrid
929 speciation in darwin's finches. *Science* 359(6372):224-228.

930 Lanfear R, Frandsen PB, Wright AM, Senfeld T, Calcott B. 2017. Partitionfinder 2: New methods for
931 selecting partitioned models of evolution for molecular and morphological phylogenetic
932 analyses. *Mol Biol Evol.* 34(3):772-773.

933 Larget BR, Kotha SK, Dewey CN, Ané C. 2010. Bucky: Gene tree/species tree reconciliation with
934 bayesian concordance analysis. *Bioinformatics* 26(22):2910-2911.

935 Larsson A. 2014. Aliview: A fast and lightweight alignment viewer and editor for large datasets.
936 *Bioinformatics* 30(22):3276-3278.

937 Lerner HR, Meyer M, James HF, Hofreiter M, Fleischer RC. 2011. Multilocus resolution of
938 phylogeny and timescale in the extant adaptive radiation of hawaiian honeycreepers. *Curr*
939 *Biol.* 21(21):1838-1844.

940 Li H. 2011. A statistical framework for snp calling, mutation discovery, association mapping and
941 population genetical parameter estimation from sequencing data. *Bioinformatics*
942 27(21):2987-2993.

943 Li H. 2013. Aligning sequence reads, clone sequences and assembly contigs with bwa-mem. arXiv
944 preprint arXiv:13033997.

945 Li H, Handsaker B, Wysoker A, Fennell T, Ruan J, Homer N, Marth G, Abecasis G, Durbin R. 2009.
946 The sequence alignment/map format and samtools. *Bioinformatics* 25(16):2078-2079.

947 Linkem CW, Minin VN, Leaché AD. 2016. Detecting the anomaly zone in species trees and evidence
948 for a misleading signal in higher-level skink phylogeny (squamata: Scincidae). *Syst Biol.*
949 65(3):465-477.

950 Lutgen D, Ritter R, Olsen RA, Schielzeth H, Gruselius J, Ewels P, García JT, Shirihai H, Schweizer M,
951 Suh A. 2020. Linked-read sequencing enables haplotype-resolved resequencing at
952 population scale. *Mol Ecol Resour.* 20(5):1311-1322.

953 Maddison WP. 1997. Gene trees in species trees. *Syst Biol.* 46(3):523-536.

954 Malinsky M, Matschiner M, Svardal H. 2021. Dsuite-fast d-statistics and related admixture
955 evidence from vcf files. *Mol Ecol Resour.* 21(2):584-595.

956 Malinsky M, Svardal H, Tyers AM, Miska EA, Genner MJ, Turner GF, Durbin R. 2018. Whole-genome
957 sequences of malawi cichlids reveal multiple radiations interconnected by gene flow. *Nat*
958 *Ecol Evol.* 2(12):1940-1955.

959 Marques DA, Lucek K, Sousa VC, Excoffier L, Seehausen O. 2019a. Admixture between old lineages
960 facilitated contemporary ecological speciation in lake constance stickleback. *Nat Commun.*
961 10(1):1-14.

962 Marques DA, Meier JI, Seehausen O. 2019b. A combinatorial view on speciation and adaptive
963 radiation. *Trends Ecol Evol.* 34(6):531-544.

964 Martin A, Orgogozo V. 2013. The loci of repeated evolution: A catalog of genetic hotspots of
965 phenotypic variation. *Evolution* 67(5):1235-1250.

966 Mayr E, Stresemann E. 1950. Polymorphism in the chat genus oenanthe (aves). *Evolution* 4:291-
967 300.

968 McKenna A, Hanna M, Banks E, Sivachenko A, Cibulskis K, Kernytsky A, Garimella K, Altshuler D,
969 Gabriel S, Daly M. 2010. The genome analysis toolkit: A mapreduce framework for
970 analyzing next-generation DNA sequencing data. *Genome Res.* 20(9):1297-1303.

971 Meier JI, Marques DA, Mwaiko S, Wagner CE, Excoffier L, Seehausen O. 2017. Ancient hybridization
972 fuels rapid cichlid fish adaptive radiations. *Nat Commun.* 8(1):1-11.

973 Meier JI, Marques DA, Wagner CE, Excoffier L, Seehausen O. 2018. Genomics of parallel ecological
974 speciation in lake victoria cichlids. *Mol Biol Evol.* 35(6):1489-1506.

975 Minh BQ, Hahn MW, Lanfear R. 2020a. New methods to calculate concordance factors for
976 phylogenomic datasets. *Mol Biol Evol.* 37(9):2727-2733.

977 Minh BQ, Schmidt HA, Chernomor O, Schrempf D, Woodhams MD, Von Haeseler A, Lanfear R.
978 2020b. Iq-tree 2: New models and efficient methods for phylogenetic inference in the
979 genomic era. *Mol Biol Evol.* 37(5):1530-1534.

980 Montejo-Kovacevich G, Meier JI, Bacquet CN, Warren IA, Chan YF, Kucka M, Salazar C, Rueda N,
981 Montgomery SH, McMillan WO. 2021. Repeated genetic adaptation to high altitude in two
982 tropical butterflies. bioRxiv.

983 Natarajan C, Projecto-Garcia J, Moriyama H, Weber RE, Muñoz-Fuentes V, Green AJ, Kopuchian C,
984 Tubaro PL, Alza L, Bulgarella M. 2015. Convergent evolution of hemoglobin function in
985 high-altitude andean waterfowl involves limited parallelism at the molecular sequence
986 level. *PLoS Genet*. 11(12):e1005681.

987 Nater A, Burri R, Kawakami T, Smeds L, Ellegren H. 2015. Resolving evolutionary relationships in
988 closely related species with whole-genome sequencing data. *Syst Biol.* 64(6):1000-1017.

989 Outlaw RK, Voelker G, Bowie RC. 2010. Shall we chat? Evolutionary relationships in the genus
990 cercomela (muscicapidae) and its relation to oenanthe reveals extensive polyphyly among
991 chats distributed in africa, india and the palearctic. *Mol Phylogenet Evol.* 55(1):284-292.

992 Panov E. 1992. Emergence of hybridogenous polymorphism in the oenanthe picata complex.
993 Bulletin of the British Ornithologists' Club Centenary Volume. 112:237-249.

994 Panov EN. 2005. Wheatears of palearctic. Pensoft.

995 Pardo-Diaz C, Salazar C, Baxter SW, Merot C, Figueiredo-Ready W, Joron M, McMillan WO, Jiggins
996 CD. 2012. Adaptive introgression across species boundaries in heliconius butterflies. *PLoS*
997 *Genet*. 8(6):e1002752.

998 Paterson RS, Rybczynski N, Kohno N, Maddin HC. 2020. A total evidence phylogenetic analysis of
999 pinniped phylogeny and the possibility of parallel evolution within a monophyletic
1000 framework. *Front Ecol Evol.* 7:457.

1001 Pease JB, Haak DC, Hahn MW, Moyle LC. 2016. Phylogenomics reveals three sources of adaptive
1002 variation during a rapid radiation. *PLoS Biol.* 14(2):e1002379.

1003 Peona V, Palacios-Gimenes O, Lutgen D, Olsen R, Alaei Kakhki N, Andriopoulos P, Bontzorlos V,
1004 Schweizer M, Suh A, Burri R. in prep. A chromosome-scale reference genome for eastern
1005 black-eared wheatear (oenanthe melanoleuca).

1006 Poelstra JW, Vijay N, Bossu CM, Lantz H, Ryll B, Müller I, Baglione V, Unneberg P, Wikelski M,
1007 Grabherr MG. 2014. The genomic landscape underlying phenotypic integrity in the face of
1008 gene flow in crows. *Science* 344(6190):1410-1414.

1009 Preston JC, Hileman LC. 2009. Developmental genetics of floral symmetry evolution. *Trends Plant*
1010 *Sci.* 14(3):147-154.

1011 Protas ME, Hersey C, Kochanek D, Zhou Y, Wilkens H, Jeffery WR, Zon LI, Borowsky R, Tabin CJ.
1012 2006. Genetic analysis of cavefish reveals molecular convergence in the evolution of
1013 albinism. *Nat Genet*. 38(1):107-111.

1014 Rambaut A, Drummond A. 2009. Tracer v1. 5.0. Available at: Http://beast.Bio.Ed.Ac.Uk/tracer.

1015 Randler C, Förschler MI, Gonzalez J, Aliabadian M, Bairlein F, Wink M. 2012. Phylogeography, pre-
1016 zygotic isolation and taxonomic status in the endemic cyprus wheatear oenanthe cypriaca.
1017 *J Ornithol*. 153(2):303-312.

1018 Roberts Kingman GA, Vyas DN, Jones FC, Brady SD, Chen HI, Reid K, Milhaven M, Bertino TS,
1019 Aguirre WE, Heins DC. 2021. Predicting future from past: The genomic basis of recurrent
1020 and rapid stickleback evolution. *Sci Adv*. 7(25):eabg5285.

1021 Ronquist F, Teslenko M, Van Der Mark P, Ayres DL, Darling A, Höhna S, Larget B, Liu L, Suchard
1022 MA, Huelsenbeck JP. 2012. Mrbayes 3.2: Efficient bayesian phylogenetic inference and
1023 model choice across a large model space. *Syst Biol.* 61(3):539-542.

1024 Roy SW. 2009. Phylogenomics: Gene duplication, unrecognized paralogy and outgroup choice.
1025 *PLoS One* 4(2):e4568.

1026 Salichos L, Stamatakis A, Rokas A. 2014. Novel information theory-based measures for quantifying
1027 incongruence among phylogenetic trees. *Mol Biol Evol.* 31(5):1261-1271.

1028 Sangster G, Alström P, Forsmark E, Olsson U. 2010. Multi-locus phylogenetic analysis of old world
1029 chats and flycatchers reveals extensive paraphyly at family, subfamily and genus level
1030 (aves: Muscicapidae). *MPE*. 57(1):380-392.

1031 Sayyari E, Mirarab S. 2018. Testing for polytomies in phylogenetic species trees using quartet
1032 frequencies. *Genes* 9(3):132.

1033 Sayyari E, Whitfield JB, Mirarab S. 2018. Discovista: Interpretable visualizations of gene tree
1034 discordance. *MPE*. 122:110-115.

1035 Schweizer M, Shirihai H. 2013. Phylogeny of the oenanthe lugens complex (aves, muscicapidae:
1036 Saxicolinae): Paraphyly of a morphologically cohesive group within a recent radiation of
1037 open-habitat chats. *MPE*. 69(3):450-461.

1038 Schweizer M, Warmuth V, Alaei Kakhki N, Aliabadian M, Förschler M, Shirihai H, Suh A, Burri R.
1039 2019a. Parallel plumage colour evolution and introgressive hybridization in wheatears. *J*
1040 *Evol biol*. 32(1):100-110.

1041 Schweizer M, Warmuth VM, Kakhki NA, Aliabadian M, Förschler M, Shirihai H, Ewels P, Gruselius
1042 J, Olsen R-A, Schielzeth H et al. 2019b. Genome-wide evidence supports mitochondrial
1043 relationships and pervasive parallel phenotypic evolution in open-habitat chats. *MPE*.
1044 139:106568.

1045 Seehausen O, Butlin RK, Keller I, Wagner CE, Boughman JW, Hohenlohe PA, Peichel CL, Saetre G-P,
1046 Bank C, Brännström Å. 2014. Genomics and the origin of species. *Nat Rev Genet.* 15(3):176-
1047 192.

1048 Simão FA, Waterhouse RM, Ioannidis P, Kriventseva EV, Zdobnov EM. 2015. Busco: Assessing
1049 genome assembly and annotation completeness with single-copy orthologs.
1050 *Bioinformatics* 31(19):3210-3212.

1051 Smith SA, Moore MJ, Brown JW, Yang Y. 2015. Analysis of phylogenomic datasets reveals conflict,
1052 concordance, and gene duplications with examples from animals and plants. *BMC Evol*
1053 *Biol.* 15(1):1-15.

1054 Song Y, Endepols S, Klemann N, Richter D, Matuschka F-R, Shih C-H, Nachman MW, Kohn MH.
1055 2011. Adaptive introgression of anticoagulant rodent poison resistance by hybridization
1056 between old world mice. *Curr Biol.* 21(15):1296-1301.

1057 Stahl BA, Gross JB. 2015. Alterations in mc1r gene expression are associated with regressive
1058 pigmentation in astyanax cavefish. *Dev Genes Evol.* 225(6):367-375.

1059 Stenz NW, Larget B, Baum DA, Ané C. 2015. Exploring tree-like and non-tree-like patterns using
1060 genome sequences: An example using the inbreeding plant species arabidopsis thaliana
1061 (l.) heynh. *Syst Biol.* 64(5):809-823.

1062 Stern DL. 2013. The genetic causes of convergent evolution. *Nat Rev Genet.* 14(11):751-764.

1063 Stryjewski KF, Sorenson MD. 2017. Mosaic genome evolution in a recent and rapid avian radiation.
1064 Nature. *Nat Ecol Evol*. 1(12):1912-1922.

1065 Suh A. 2016. The phylogenomic forest of bird trees contains a hard polytomy at the root of
1066 neoaves. *Zoologica Scripta* 45:50-62.

1067 Suh A, Smeds L, Ellegren H. 2015. The dynamics of incomplete lineage sorting across the ancient
1068 adaptive radiation of neoavian birds. *PLoS Biol.* 13(8):e1002224.

1069 Swofford D. 2003. Paup*. Phylogenetic analysis using parsimony (*and other methods). Version 4
1070 Sinauer Associates, Sunderland, Massachusetts.

1071 Tamura K, Stecher G, Kumar S. 2021. Mega11: Molecular evolutionary genetics analysis version
1072 11. *Mol Biol Evol.* 38(7):3022-3027.

1073 Than C, Ruths D, Nakhleh L. 2008. Phylonet: A software package for analyzing and reconstructing
1074 reticulate evolutionary relationships. *BMC bioinformatics* 9(1):1-16.

1075 Toews DP, Brelsford A. 2012. The biogeography of mitochondrial and nuclear discordance in
1076 animals. *Mol Ecol.* 21(16):3907-3930.

1077 Van Belleghem SM, Vangestel C, De Wolf K, De Corte Z, Möst M, Rastas P, De Meester L, Hendrickx
1078 F. 2018. Evolution at two time frames: Polymorphisms from an ancient singular
1079 divergence event fuel contemporary parallel evolution. *PLoS Genet*. 14(11):e1007796.

1080 Van Damme K, Cornetti L, Fields PD, Ebert D. 2022. Whole-genome phylogenetic reconstruction
1081 as a powerful tool to reveal homoplasy and ancient rapid radiation in waterflea evolution.
1082 *Syst Biol.* 71(4):777-787.

1083 Vaughan TG. 2017. Icytree: Rapid browser-based visualization for phylogenetic trees and
1084 networks. *Bioinformatics* 33(15):2392-2394.

1085 Wallbank RW, Baxter SW, Pardo-Diaz C, Hanly JJ, Martin SH, Mallet J, Dasmahapatra KK, Salazar C,
1086 Joron M, Nadeau N. 2016. Evolutionary novelty in a butterfly wing pattern through
1087 enhancer shuffling. *PLoS Biol*. 14(1):e1002353.

1088 Whittall JB, Voelckel C, Kliebenstein DJ, Hodges SA. 2006. Convergence, constraint and the role of
1089 gene expression during adaptive radiation: Floral anthocyanins in aquilegia. *Mol Ecol.*
1090 15(14):4645-4657.

1091 Yu Y, Dong J, Liu KJ, Nakhleh L. 2014. Maximum likelihood inference of reticulate evolutionary
1092 histories. *PNAS*. 111(46):16448-16453.

1093 Yu Y, Nakhleh L. 2015. A maximum pseudo-likelihood approach for phylogenetic networks. *BMC*
1094 *Genom*. 16(10):1-10.

1095 Zhang C, Rabiee M, Sayyari E, Mirarab S. 2018. Astral-iii: Polynomial time species tree
1096 reconstruction from partially resolved gene trees. *BMC bioinformatics* 19(6):15-30.

1097 Zuccon D, Ericson PG. 2010. A multi-gene phylogeny disentangles the chat-flycatcher complex
1098 (aves: Muscicapidae). *Zoologica Scripta* 39(3):213-224.

1099

1100

1101 **Figure captions**

1102 **Figure 1 | Time-calibrated phylogenetic tree of open-habitat chats and levels of ILS.** All
1103 nodes are supported by bootstrap values of 100. Pie charts depict the gene tree heterogeneity for
1104 each internal branch, with the brown proportion indicating the proportion of concordant gene
1105 trees (gCF). Coloured branches indicate internal branches for which ILS alone is statistically
1106 sufficient to explain the observed gene tree heterogeneity. Stars indicate branches that are in the
1107 phylogenetic anomaly zone. The character states of three selected characters: Sexual dimorphism
1108 (SD), monomorphic female-type (white), monomorphic male-type (pale green), dimorphic (dark
1109 green); Migratory behaviour (Mig), sedentary (white), short-distance migrant (pale green), long-
1110 distance migrant (dark green); and throat coloration (throat), white (white), black (pale green),
1111 and polymorphic (white and pale green). Drawing courtesy of Chris Rose (www.chrisrose-
1112 artist.co.uk) with permission from Bloomsbury Publishing Plc.

1113 **Figure 2 | Mito-nuclear discordances.** Shown are the time-calibrated phylogenetic trees based
1114 on nuclear data (left) and full mitogenomes (right).

1115 **Figure 3 | Footprints of introgression as estimated by the f-branch statistic.** The heat map
1116 summarizes the f-branch statistics estimated in Dsuite. Darker colors depict increasing evidence
1117 for gene flow between lineages. Dotted lines in the phylogeny represent ancestral lineage.

1118 **Figure 4 | Phylogenomic networks and distribution ranges for the *picata* (left), *lugens***
1119 **(middle) and *hispanica* (right) complexes.** Phylogenomic networks were estimated under the
1120 maximum pseudolikelihood approach implemented in phyloNet. Numbers on the edges indicate
1121 the inheritance probabilities, which correspond to the proportion of gene trees supporting the
1122 reticulate relationship. Drawings courtesy of Chris Rose (www.chrisrose-artist.co.uk) with
1123 permission from Bloomsbury Publishing Plc. Distribution ranges modified from BirdLife
1124 International and the Handbook of the Birds of the World (2016).

1125

1126

1127

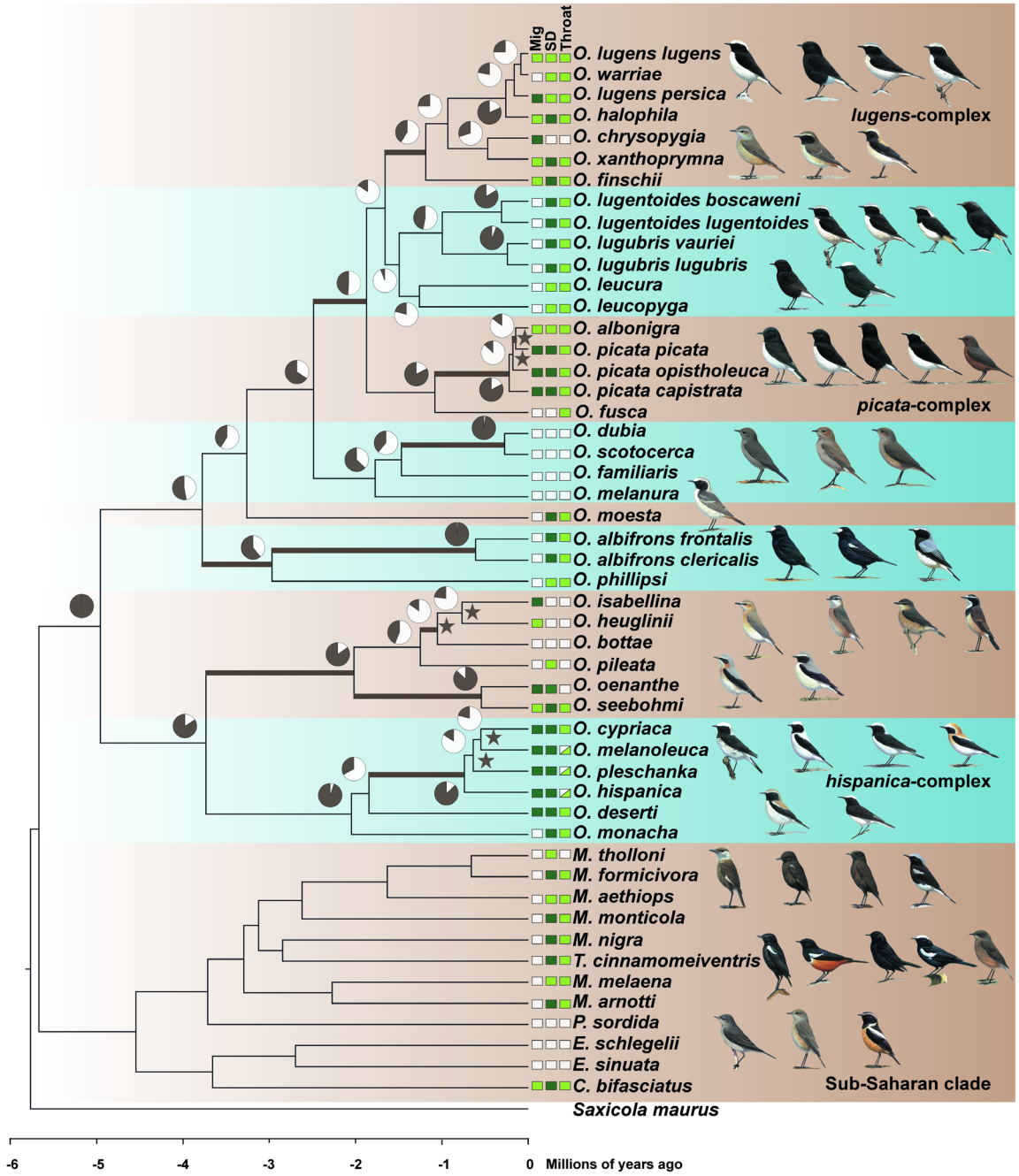

Figure 1 | Time-calibrated phylogenetic tree of open-habitat chats and levels of ILS. All nodes are supported by bootstrap values of 100. Pie charts depict the gene tree heterogeneity for each internal branch, with the brown proportion indicating the proportion of concordant gene trees (gCF). Coloured branches indicate internal branches for which ILS alone is statistically sufficient to explain the observed gene tree heterogeneity. Stars indicate branches that are in the phylogenetic anomaly zone. The character states of three selected characters: Sexual dimorphism (SD), monomorphic female-type (white), monomorphic male-type (pale green), dimorphic (dark green); Migratory behaviour (Mig), sedentary (white), short-distance migrant (pale green), long-distance migrant (dark green); and throat coloration (throat), white (white), black (pale green), and polymorphic (white and pale green). Drawing courtesy of Chris Rose (www.chrisrose-artist.co.uk) with permission from Bloomsbury Publishing Plc.

1128

1129

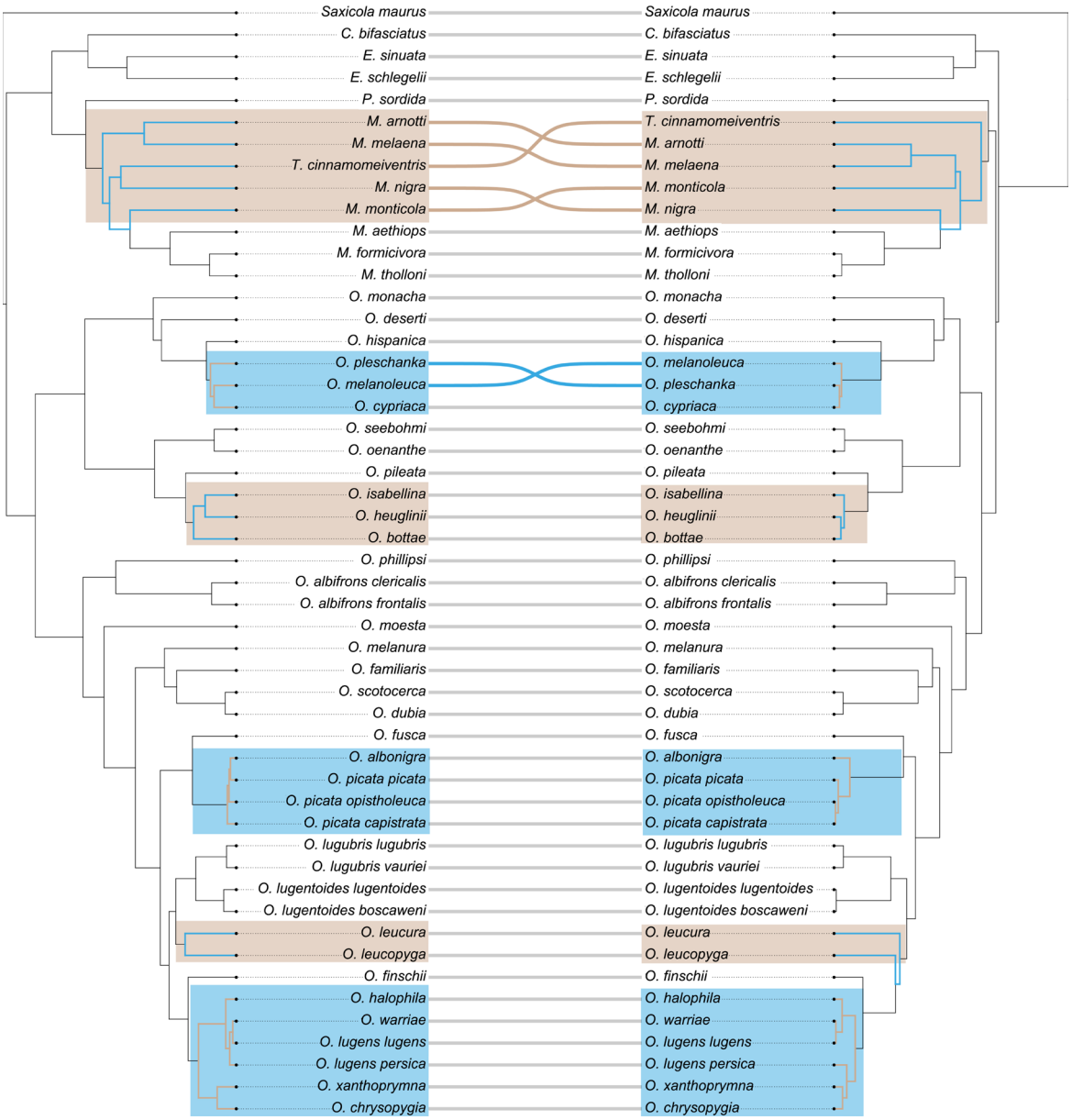

Figure 2 | Mito-nuclear discordances. Shown are the time-calibrated phylogenetic trees based on nuclear data (left) and full mitogenomes (right).

Figure 3 | Footprints of introgression as estimated by the f-branch statistic. The heat map summarizes the f-branch statistics estimated in Dsuite. Darker colors depict increasing evidence for gene flow between lineages. Dotted lines in the phylogeny represent ancestral lineage.

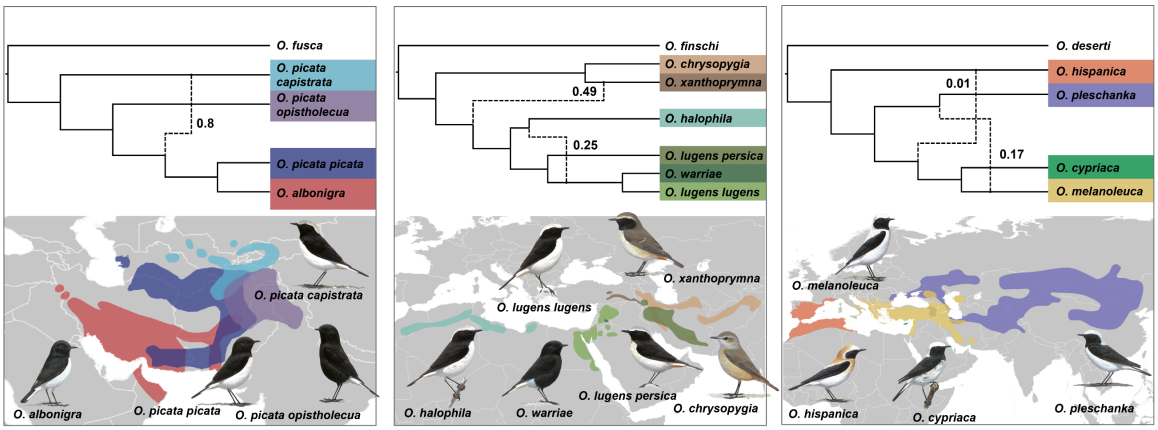

Figure 4 | Phylogenomic networks and distribution ranges for the *picata* (left), *lugens* (middle) and *hispanica* (right) complexes. Phylogenomic networks were estimated under the maximum pseudolikelihood approach implemented in phyloNet. Numbers on the edges indicate the inheritance probabilities, which correspond to the proportion of gene trees supporting the reticulate relationship. Drawings courtesy of Chris Rose (www.chrisrose-artist.co.uk) with permission from Bloomsbury Publishing Plc. Distribution ranges modified from BirdLife International and the Handbook of the Birds of the World (2016).